Bioresource Technology Reports 23 (2023) 101523

Contents lists available at ScienceDirect

Bioresource Technology Reports

journal homepage: www.sciencedirect.com/journal/bioresource-technology-reports

Scaling-up of oxygenic photogranular system in selective-CSTR

Joseph G. Gikonyo *, Ahmed S. Abouhend, Andrew Keyser, Yanwen Li, Chul Park

Department of Civil and Environmental Engineering, University of Massachusetts, Amherst, MA 01003, USA

ARTICLE INFO

Keywords:
Continuous stirred-tank reactors
Scaling-up
Granulation
Oxygenic photogranules
Internal settlers
Sustainable wastewater treatment

ABSTRACT

The light driven oxygenic photogranule process presents potential aeration free wastewater treatment. Earlier attempts to scale up OPG in larger and deeper sequencing batch reactors were found difficult due to reduced light availability arising from slug entries of turbid wastewater and the accumulation of light-attenuating small biomass. Here, we investigated the use of surface-lit 120 L selective continuous stirred-tank reactors with an internal settler to treat municipal wastewater. The internal settler was deployed to continuously remove small, slow-settling biomass and enhance light availability within the reactor. This continuous-flow OPG system achieved mean effluent TSS of 32 ± 22 mg/L and soluble COD of 31 ± 14 mg/L. A similar reactor operated for 154 days had mean effluent TSS of 28 ± 24 mg/L and soluble COD of 38 ± 17 mg/L. More notably, granulation was maintained and propagated during the operation. Overall, high yields, 0.98 and 0.81 gCOD produced/gCOD consumed were achieved for reactor R1 and R2, respectively.

1. Introduction

Wastewater treatment plants (WWTPs) are resource rich nodes with recovery potential as part of integrated circular economies (Puyol et al., 2017; Smol, 2022). Current research and industrial efforts at achieving energy neutrality, nutrients recovery, carbon diversion, emergent contaminants removal, water reuse, and biosolids reuse are testament to this need (Ali et al., 2022; Mannina et al., 2021; Smol, 2022). Moreover, the global need for WWTP solutions to increase access to sanitation globally and protect water supplies has been widely highlighted (Obaideen et al., 2022). The engineering of wastewater resource recovery facilities (WRRF) must thus keep evolving to surmount novel and accrued needs.

A crucial development in the contemporary engineering of WRRF has been the advent of aggregated biomass technologies as an alternative to the grandfather activated sludge (AS) process (Gu et al., 2017; Gurung et al., 2018; Trapote et al., 2014). Granules are dense, spherical aggregations of self-immobilized biofilms formed in the absence of solid substratum (Jimenez et al., 2020). Granular systems have reported advantages, including better solids separation, resilience to toxic loading, lower operation cost, enhanced carbon capture, reduced footprint, process intensification and enhanced contaminant removal (Gikonyo et al., 2022; Regmi et al., 2022; Rosa-Masegosa et al., 2021; Xu et al., 2022). However, knowledge gaps of the granulation mechanism and operational limitations inhibit greater engineering application (Gikonyo et al., 2021a; Park and Takeuchi, 2021; Xu et al., 2022).

Oxygenic photogranules (OPGs) are a promising granule-based biotechnology with potential to treat wastewater without aeration, which currently incurs 30–80 % of energy demand in wastewater treatment (Abouhend et al., 2018; Ansari et al., 2019; Smetana and Grosser, 2023). The OPGs are formed by a diverse microbial consortium enmeshed in extracellular polymeric substances (EPS) conferring functional modularity (Smetana and Grosser, 2023). Illumina MiSeq DNA sequencing analyses revealed that photogranulation occurs with dominant enrichment of subsection III filamentous cyanobacteria (Milferstedt et al., 2017), which possess motility (Whitman et al., 2015). In addition to filamentous cyanobacteria, microbial groups that are useful for wastewater treatment are harbored in OPGs. These include nitrifying and denitrifying bacteria and polyphosphate accumulating organisms (Abouhend et al., 2023; Milferstedt et al., 2017; Stauch-White et al., 2017).

The advent of granular morphology has been reported to arise with selection pressures induced by shear, hydraulic selection, and feast-famine conditions (Gikonyo et al., 2021a; Park and Takeuchi, 2021; Qin et al., 2004; Rosa-Masegosa et al., 2021). Despite its numerous benefits, granular reactors' operation is primarily in upflow, and sequencing batch reactor (SBR) modes engineered to foster these stresses. Unfortunately, these operational schemes impose flow exchange limited biomass inventories and flow capacity limitations (Rosa-Masegosa et al., 2021), while most granular systems require aeration,

* Corresponding author: jgikonyo@umass.edu
E-mail address: jgikonyo@umass.edu (J.G. Gikonyo).

https://doi.org/10.1016/j.biteb.2023.101523
Received 9 April 2023; Received in revised form 23 June 2023; Accepted 24 June 2023
Available online 29 June 2023

preserving high energy consumption typical of AS (Jimenez et al., 2020). In addition, high capital outlays maybe necessary to transition from conventional continuous flow reactors (CFR) operated as continuous stirred-tank reactors (CSTR) (Kent et al., 2018; Rosa-Masegosa et al., 2021).

One selection pressure rationale against CSTR operations is that steady-state conditions typical of these operations result in uniform substrate concentrations, equal to that of effluent; hence, no substrate gradient is established. Subsequently, the mass flux by diffusion will be significantly limited, restricting the growth of these self-immobilized biofilms (Kent et al., 2018). Furthermore, conventional CSTR operations do not induce hydraulic selection pressures (HSP) to retain aggregated biomass (Rosa-Masegosa et al., 2021). Consequently, granular based continuous flow reactor (CFR) designs seek to induce selection pressures essential for granulation (Ahmad et al., 2017; Bindhu and Madhu, 2016; He et al., 2018; Liu and Tay, 2015; Qin et al., 2004). Rosa-Masegosa et al. (2021) and Kent et al. (2018a) provide a detailed summary of present efforts to operate aerobic granular sludge (AGS) in CFR systems. Xu et al. (2022) provides a review of research gaps for long term AGS-CFR systems. Primarily, these CFRs employ settling velocity selection mechanisms to enhance retention of rapidly-settling biomass (Kent et al., 2018; Smetana and Grosser, 2023). Such strategies include internal and external separators, such as baffles and sieves, multi-chambered reactor systems, use of clarifiers, integrated SBR-CFR system, and AGS-membrane bioreactor. Regmi et al. (2022) recently reported successful full-scale operations of granular systems in a plug-flow based CFR using an external hydrocyclone selector. Structural stability of granules in CFRs strongly dependent on the selection pressures has been reported albeit without long-term (<100 days) stability evaluation (Xu et al., 2022).

Feast-famine selection pressure is inherent in SBR operations (Zhang et al., 2017), with advective mass transport distributing substrates in bulk fluid and substrate diffusion gradients into the granular matrix (Gikonyo et al., 2022; Wilén et al., 2018). Aggregation of microbes during famine conditions is thought to improve survival and is characterized by enhanced EPS production (Kent et al., 2018). CFR systems utilizing serial multiple chambers, reverse flows, and intermittent feeding strategies reported improved settleability of biomass arising from substrate cycling. This tapered substrate gradient is typical of PFR-CFRs reported to have granulation successes (Regmi et al., 2022; Rosa-Masegosa et al., 2021).

Shear pressure in granular systems serves to suspend the biomass and distribute bulk substrate flux (Gikonyo et al., 2021a). Shear is also crucial for sizing and 'shaping' granules, with a direct correlation to aggregates' physical attributes (Abouhend et al., 2023; Chen et al., 2007; Liu and Tay, 2002). Shear force not only increases hydrophobicity and particle density but also abets initiation and enhancement of particle collisions in the bulk fluid (Sengar et al., 2018). In granular CFRs, mixing is induced by mechanical stirrers or air flow from air diffusers and can be applied selectively to facilitate biomass separation based on settling velocity (Rosa-Masegosa et al., 2021). Induced hydraulic circulation can result in filamentous entanglement akin to observed fungal pelletization (Kent et al., 2018).

Despite successful demonstration of OPGs in bench-scale SBR treating real wastewater (Abouhend et al., 2018), reported attempts to scale up OPGs in SBR have failed (McNair, 2017), and unreported numerous follow-ups attempts with SBR in the authors' laboratory also failed. It was commonly observed that despite initial success, septic conditions soon developed indicating limitation in photosynthetic activity. This occurred with the loss of granular biomass and the loss of system functionality. There have been few reports on the use of CFR for OPGs or other photogranular moieties. Safitri et al. (2021) reported the bench-scale operation of OPG in continuous flow conditions in a manner alike an upflow anaerobic sludge blanket (UASB) reactor. A bench-scale algal-bacterial aggregate CFR system operated at 2-day hydraulic retention time (HRT) was reported, with high floc persistence in larger 600 L reactor compared to 30 L system (Gutzeit et al., 2005).

It was postulated that OPGs can functionally persist in CFRs, and the operation of OPGs in selective-continuous stirred-tank reactors (sCSTR) would foster scaling-up for wastewater treatment. The cycling of critical substrates for OPGs' microbial groups, O_2 and organic matter (also as the source of CO_2), is intra-granular, hence supporting microbes within the granules even in low diffusion-flux CSTR operation. Selective retention of larger granules by internal settlers was hypothesized to increase inter-granular spaces, favoring higher light penetration. Furthermore, we hypothesized that the entry of wastewater in continuous mode instead of slug feeding as well as the continuous reactions contributing to the development of (quasi) steady-state conditions would facilitate a clear water background, significantly enhancing photosynthesis by OPGs and maintaining the system functions. This work reports the sCSTR operation strategies in OPG scaleup for treating solids-laden real wastewater without energy intensive aeration.

2. Materials and methods

2.1. Reactor seeding

OPGs for seeding the reactors were generated as previously described by authors (Gikonyo et al., 2021a). Briefly, activated sludge collected from the local utility was incubated under hydrodynamic conditions for 8 days. The inoculum was first diluted four times and transferred to 1 L jars. The 6 jars were then mixed at 30 rpm and illuminated with 150–210 μmol/m^2-s continuously for the duration. Harvested biomass matrices were passed through a 200 μm sieve via the wet sieve method (Abouhend et al., 2020), with recovery of OPG granules >200 μm. The granules were then seeded into reactor R1. Reactor R2 on the other hand was seeded with biomass harvested from reactor R1 on day 272.

2.2. Reactor operation

A tank reactor of 0.47 m × 0.62 m × 0.5 m (L × W × H) was set up with a working volume of 120 L and fitted with an overhead mixer (IKA® RW20). The mixer was operated at 50 rpm for both reactors R1 and R2. Mixing in these continuous-flow reactors utilized pitched blade impellers inducing a theoretical shear stress of 0.06 N/m^2, a velocity gradient G of 62.6 s^{-1}, and Kolmogorov length scale of 126 μm (Video 1 attached). Mixing in reactor R2 was increased to 80 rpm from day 112 increasing the shear stress by 112 % while lowering the Kolmogorov scale to 89 μm. Light was provided using LED panels (daylight- 5000 K) located to provide 413 ± 53 μmol/m^2-s at the water surface. During the initial 36 days period, reactor R1 was operated with 4–6 h periods of dark as a suspended growth control strategy. The reactor HRT and solids retention times (SRT) was managed in response to reactor conditions.

Reactor influent stream was drawn from the WWTP primary effluent flow splitter box. This feed had a mean total suspended solids (TSS) of 64 ± 39 mg/L and the ratio of volatile suspended solids (VSS) to TSS (VSS/TSS) of 0.84 ± 0.12. The influent total chemical oxygen demand (tCOD), and soluble COD (sCOD) were 177 ± 77 mg/L and 60 ± 22 mg/L, respectively. Total dissolved nitrogen (TDN) was found to have a mean of 13 ± 4.5 mg/L. pH in the two reactors was between 6.8 and 7.6 for the duration of operation. The operation was undertaken under a pvc canopy with temperature amendment during winter. Overflow incidences, resulting in some losses in biomass were experienced on day 7, day 132, and day 197 for reactor R1 and on day 42 for reactor R2.

2.3. Internal settler design

During the continuous flow operation, an internal settler was utilized to facilitate biomass separation by allowing upflow uptake of solids and effluent from the bulk stream while fast-settling biomass settled out. This hydraulic selection pressure (HSP) facilitated accumulation of fast settling granular biomass and effectively pulled out small particles.

Removal of these smaller particles facilitates light penetration by reducing particle interference. During the initial 36 days of R1 operation, a settler with 16.7 cm diameter (denoted as S_A) and 1 L working volume was used. This provided a 12 min detention time and a 5.5 $m^3/m^2/d$ overflow rate through the internal settler for a 1-d HRT (Table 1). Subsequent operation for both R1 and R2 was undertaken with a 4.2 cm diameter settler (denoted as S_B) at different volume configurations. The internal settler overflow rates ($m^3/m^2/d$), retention times (m), reactor HRTs (d), and corresponding settler volumes (L) used during this period are presented in Table 1. The settler volume was adjusted to investigate the biomass retention impacts on reactor operation. The upflow velocity of bulk fluid in the reactor was determined as,

$$Upflow\ Velocity\left(\frac{m}{hr}\right) = \frac{Volume}{Cross-sectional\ Area*HRT} \quad (1)$$

where, volume (m^3) and cross-sectional area (m^2) are reactor parameters.

The reactor effluent-1 continually eluted from this internal settler was subsequently settled for 15 min giving an effluent-2 stream. While the 15-min settling time was arbitrary, higher retention time to eliminate more solids could be undertaken during secondary clarification.

2.4. Sample analysis

Influent, reactor bulk (i.e., mixed liquor), and effluent samples were collected frequently during the study. TSS and VSS of these samples were measured using Standard Methods 2540D/E (APHA, 2012). Influent and effluent samples were evaluated for tCOD and filtered through 0.45 μm filters for analysis of sCOD fractions, using Standard Methods 5220D (APHA, 2012). The 0.45 μm filtrate was further evaluated for soluble fractions of total dissolved nitrogen (TDN) and dissolved organic carbon using a TN/TOC analyzer (TOC-VCPH, Shimadzu, Japan). Extraction and quantification of chlorophyll pigments were undertaken using Standard Methods 10200H (APHA, 2012). Phycobilisomes (PBS), cyanobacterial light harvesting complex accessory pigments, were quantified as previously outlined by the authors (Gikonyo et al., 2021a). Briefly, 10 mL samples were centrifuged at 15000 rpm, extraction done with phosphate buffer solution at pH 7.2, and quantification done using the Bennett and Bogorad equations with protein unique absorbances (Lauceri et al., 2017).

The sludge volume index (SVI) after 5 min and 30 min settling of the reactor's biomass, SVI_5 and SVI_{30}, was determined based on Standard Methods (2710D/E) (APHA, 2012), and their ratio was obtained—An SVI_5/SVI_{30} ratio of 1.0 coupled with low SVI_5 would indicate good granulation with fast settling biomass. Dissolved oxygen (DO), oxidation reduction potential (ORP), and pH were monitored in real time using an Orion™ Versa Star Pro™ meter and probes (Thermo Scientific). Light calibrations and dissipation were monitored using a Li-Cor 193S underwater spherical sensor (LI-COR Biosciences).

Biomass yields and SRT were enumerated retrospectively. The linear regression observed yields (Y_{obs}) for different periods are presented as g tCOD produced/g tCOD consumed. A gCOD/gVSS conversion for OPG of 1.8 ± 0.09 presented by Abouhend et al. (2018) was used.

Table 1
Internal settler parameters for operation period with internal settler S_A and S_B in reactor R1 and settler S_B in reactor R2. The operation code indicates the settler–HRT (d)–settler volume (L).

Operation code	HRT (d)	Settler volume (L)	Overflow rate ($m^3/m^2/day$)	Upflow velocity (m/h)	Settler retention time (min)
$S_{A\text{-}1d\text{-}1L}$	1	1	5.5	10.1	12
$S_{B\text{-}1d\text{-}1L}$	1	1	86.6	10.1	12
$S_{B\text{-}1d\text{-}0.5L}$	1	0.5	86.6	10.1	6
$S_{B\text{-}0.75d\text{-}0.75L}$	0.75	0.75	115.5	13.4	6.75
$S_{B\text{-}0.75d\text{-}0.5L}$	0.75	0.5	115.5	13.4	4.5
$S_{B\text{-}0.75d\text{-}0,25L}$	0.75	0.25	115.5	13.4	2.25
$S_{B\text{-}0.5d\text{-}0.75L}$	0.5	0.75	173.3	20.1	4.5
$S_{B\text{-}0.5d\text{-}0.5L}$	0.5	0.5	173.3	20.1	3
$S_{B\text{-}0.5d\text{-}0.25L}$	0.5	0.25	173.3	20.1	1.5
$S_{B\text{-}0.33d\text{-}0.5L}$	0.33	0.5	262.5	30.5	2
$S_{B\text{-}0.25d\text{-}0.5L}$	0.25	0.5	346.5	40.3	1.5

2.5. Microscopy

Light microscopy (EVOS FL Color AMEFC-4300) was conducted using bright field and epifluorescence (RFP light cube-532 excitation/590 Emission) to characterize morphology and microbial composition. Cyanobacterial enrichment expected with OPG granulation results in golden-orange fluorescence due to the cyanobacteria's light harvesting complex proteins, specifically phycoerythrin (Gikonyo et al., 2021a). A 50 mL biomass duplicate sample was used to acquire high resolution petri dish images, and Image pro®v10 software (MEDIA CYBERNETICS) was utilized to characterize evolution of particle sizes and number.

2.6. Statistical analysis

Statistical analysis on reactor parameter was undertaken using Microsoft Excel 365 and OriginPro 2022 (©Origin Lab Corporation). Particle size characteristics were modelled using a Weibull and Lognormal distributions and model of fit evaluated using the Kolmogorov-Smirnov test. Spearman's test was used to evaluate correlation between variables with a 2-tail significance test and presented at r (n minus 2) = r statistic, and p = *p*-value. Analysis of variance (ANOVA) for single and two factors was used to analyze the effect of HRT and settler volume on the removal efficiency (% COD, % TDN) from the OPG reactors. Post hoc evaluation of significant differences was undertaken using the Bonferroni test while all tests were made under a significance level ($p = 0.05$) and a minimum number of replicates ($n = 2$) for each analyzed variable.

3. Results

3.1. Reactor R1 with internal settlers S_A and S_B

3.1.1. Reactor R1 with internal settler S_A

Operating the R1 with a large surface area internal settler S_A (day 0 to day 36) resulted in increasing biomass inventories from 80 to 1160 mg/L (Fig. 1a). After an initial decrease, an increase in effluent-1 solids concentration (mean 55 ± 22 mg/L) resulted in increasing MLSS (Fig. 2a). The increasing effluent-1 TSS is indicative of robust removal of slow settling biomass through the internal settler. An initial increase in sCOD was followed by a decrease from a peak of 63 mg/L and the mean effluent sCOD during this period was 22 ± 17 mg/L (Fig. 3a). The observed yield during this period was 0.63 gCOD produced/gCOD consumed and the mean SRT was 7 days (Table 2). Mean particle diameter increased by 48 % from 0.82 ± 0.35 mm on day 0 to 1.2 ± 0.63 mm on day 36, while median particle sizes initially decreased by 12 % from initial 0.76 mm, suggesting shear modified growth. Increased shear environments erode particle surfaces decreasing sizes (Abouhend et al., 2023). By day 36 the maximum particle sizes increased by 52 % to 3.17 mm (Fig. 4a). This size increase can be attributed to particle attachment and enmeshment occurring during aggregation that eases growth of biomass beyond the shear limited size (Abouhend et al., 2023; Gikonyo et al., 2021a). However, the particle size distribution mode was conserved at 0.49 mm during this period. Concurrently, the SVI_5 increased from 125 mL/g at start to SVI_5 of 1573 ± 1283 mL/g (SVI_5/SVI_{30} = 5.3) by day 36 (Fig. 5a), indicating retrogressing settleability (Gikonyo et al., 2021a).

An initial temporal increase of chlorophyll pigments was observed

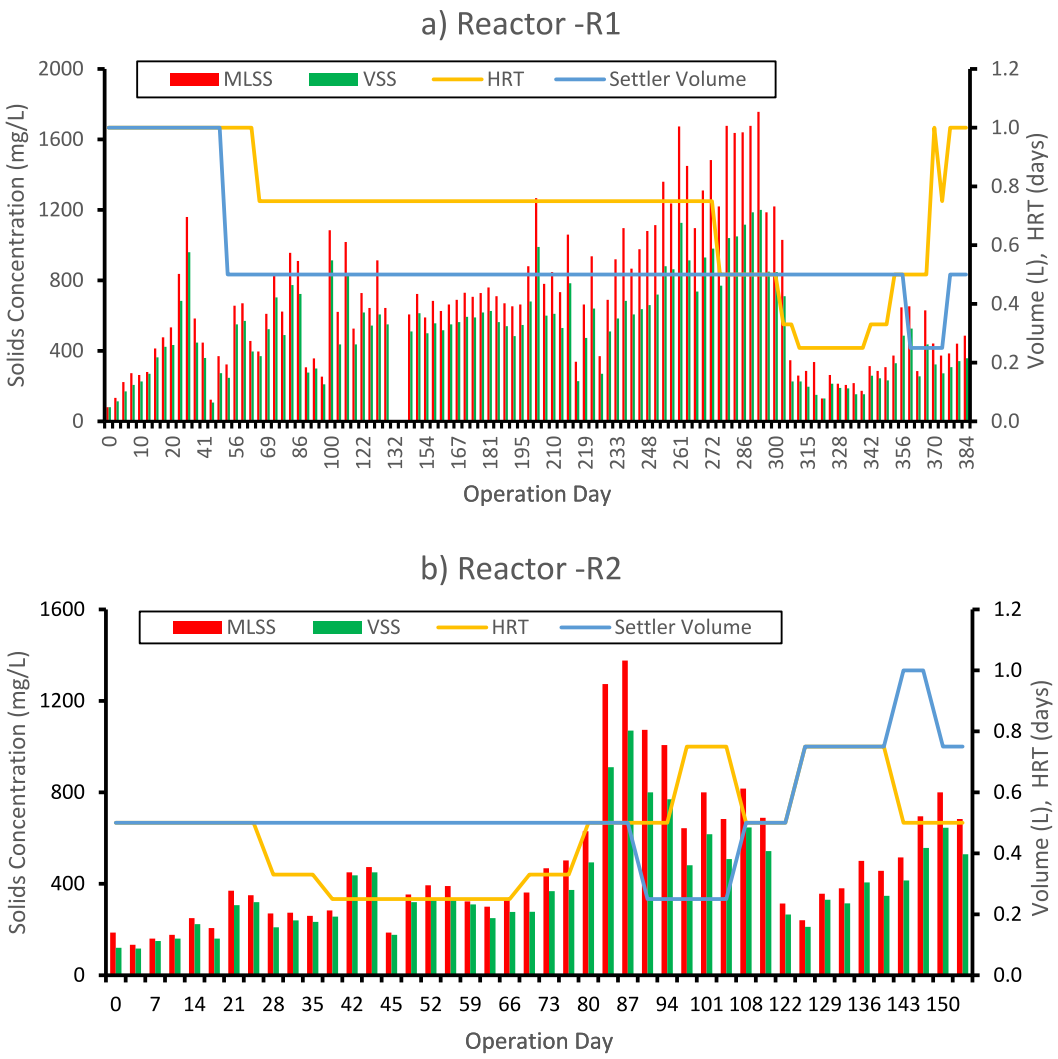

Fig. 1. Biomass concentrations and operational parameters deployed for OPG sCSTR reactor (a) R1 and (b) R2. MLSS (mg/L): mixed liquor suspended solids. VSS (mg/L): volatile suspended solids. HRT: hydraulic retention time (d) of reactors. Settler volume (L): volume of internal settler in reactors.

(Fig. 6a) followed by decreasing concentrations during this operational period. Phycobilisomes (PBS) concentrations initially increased to day 6 (Fig. 6b) thereafter decreasing to day 36. The initial increases in pigments' concentrations suggests an accretion of phototrophs characteristic of OPGs and well-lit reactor environment while later decreases in pigment levels allude to growth limitations. Concurrently, an 85–91 % decrease in light penetration, from 83 μmol/m^2-s to 9 μmol/m^2-s, within the reactor at a depth of 7 cm below the water surface ensued, leading to reactor darkening. Notwithstanding the increase in biomass concentration, accumulation of small particles with low settling velocities and inhibiting light penetration, and decreasing phototrophic moieties was deemed ill-suited for OPG operation. Consequently, we undertook a change of the internal settler to increase the operational surface overflow rate and decrease the settler retention time from 12 min (Table 1).

3.1.2. *Reactor R1 with internal settler S_B*

The primacy of HSP for granulation has been widely reviewed by Kent et al. (2018). SBR with long settling times >30 min did not enhance granulation albeit presence of other selection pressures. The Nereda process utilizing long settling selection and deep reactors is an outlier to this observation (Kent et al., 2018). The ease of applying settling based selection in SBR operations befits its application for granular based wastewater treatment in contrast to CSTR operations. Settling time applied for granulation is thus substantially shorter than typical sludge settling time used in the activated sludge process, such as 2–3 h. A smaller surface area settler (S_B), with lower retention time and higher surface overflow rates (Table 1), thus provided stronger HSP in this system, and small or light particles were continuously pulled out of this selective OPG CSTR system. Light conditions within the reactor-measured at 7 cm below surface improved to between 32 μmol/m^2-s and 102 μmol/m^2-s for the duration of this operation.

3.1.2.1. Operation at 1 d HRT, 1 L and 0.5 L internal settler volumes. Increasing the overflow rate with settler S_B and 1-d HRT ($S_{B\text{-}1d\text{-}1L}$) (day 37 to day 51) resulted in a decrease of biomass inventory to 329 ± 151 mg/L by day 51 (Fig. 1a). The average VSS/MLSS ratio during this period decreased to 0.79 from 0.85 in the earlier period (Fig. 1a). Effluent-1 TSS increased by 63 % from the preceding operation to a mean of 89 ± 16 mg/L (Fig. 2a). Similarly, the sCOD in effluent during this period increased by 48 % to a mean of 32 ± 9 mg/L and Y_{obs} of 0.46 gCOD produced/gCOD consumed (Table 2) was observed. The COD removal efficiency decreased during this period, which can be ascribed to higher overflow rate (Table 1). The corresponding low yield also reflects low productivity related to robust removal at this higher settler overflow rates. Meanwhile, SVI_5 decreased to 169 ± 60 mL/g with an SVI_5/SVI_{30} ratio of 4.9 (Fig. 5a) during this period, and mean particle size increased to 1.29 ± 1.17 mm with an unchanged mode of 0.49 mm (Fig. 4a). A higher maximum particle size, 4.69 mm, was also observed

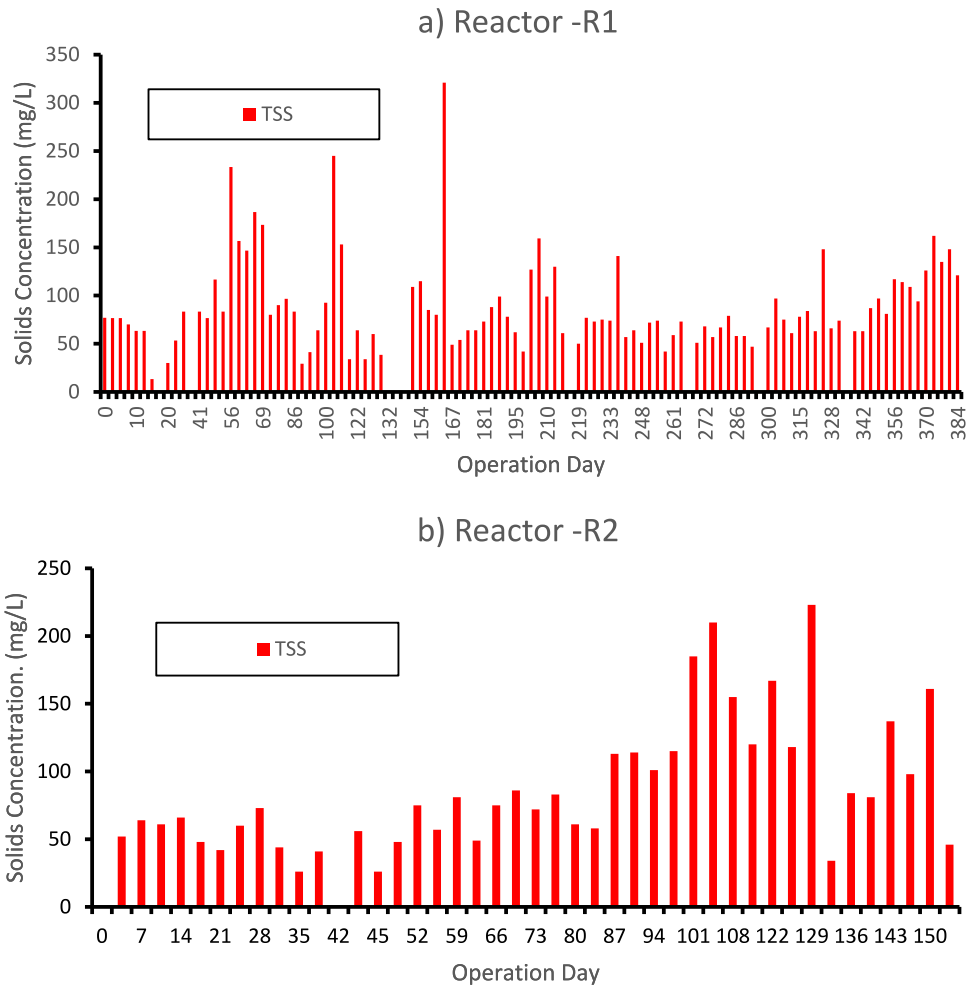

Fig. 2. Effluent-1 TSS (mg/L) of OPG sCSTR reactors (a) R1 and (b) R2.

on day 51 compared to day 31. Total dissolved nitrogen (TDN) removal efficiency increased by 71 % with this configuration as compared to operation with settler S_A (Fig. S2a).

Further, decreasing the settler retention time to 6 min ($S_{B\text{-}1d\text{-}0.5L}$) up to day 65, resulted in MLSS increases to a mean of 531 ± 120 mg/L with a VSS/MLSS ratio of 0.87 (Fig. 1a). Mean effluent-1 TSS doubled while sCOD removal increased by 13 % to a mean of 28 ± 4 mg/L (Fig. 2a, Fig. 3a). This period resulted in a 52 % increase of Y_{obs} (0.7 gCOD produced/gCOD consumed) (Table 2). While maximum and dominant particle sizes remained largely unchanged from previous settler setting, the mean particle sizes decreased by 17 % to 1.08 ± 0.97 mm. The resulting mean SVI_5 for this configuration was 130 ± 19 mL/g (Fig. 5a), an 18 % decrease compared to operation at higher retention time. Halving the internal settler retention time from 12 to 6 min enhanced solids removal, increasing the food to microorganism's ratio (F:M) and enhancing growth within the reactors. This rapid growth of biomass was characterized by proliferation of both algae and diatoms as evidenced by increasing concentrations of chlorophyll-b and chlorophyll-c (data not shown), with decreasing total chlorophyll (Fig. 6a) and phycobilins pigments (Fig. 6b). The biomass productivity could also be attributed to high heterotrophic growth comparable to high-rate activated sludge processes (Canals et al., 2023). A mean TDN removal of 3.0 mg/L, a 19 % removal efficiency, was seen (Fig. S2a) for this $S_{B\text{-}1d\text{-}0.5L}$ configuration. Eluting biomass, especially rapidly propagating small granules (Abouhend et al., 2018, 2020), decreases the functional efficiency of the OPG sCSTR reactor. During this period, OPGs with a halo of ciliates were observed (Fig. 7c) with this morphology attributed to high DO concentrations established in the reactor (data not shown).

3.1.2.2. Operation at 0.75 d HRT and 0.5 L internal settler volume. To counter the high DO concentrations in the reactor (up to 5.8 mg/L) during operations with $S_{B\text{-}1d\text{-}0.5L}$, HRT was decreased to 0.75 d ($S_{B\text{-}0.75\ d\text{-}0.5L}$) from day 66 till day 272, decreasing retention time within the settler to 4.5 min at an overflow rate of 115.5 $m^3/m^2/d$ (Table 2). This 33 % increase in HSP resulted in increased MLSS to 771 ± 299 mg/L (Fig. 1). Effluent-1 TSS decreased to 75 ± 51 mg/L (Fig. 2a) and sCOD was 31 ± 11 mg/L (Fig. 3a). A second effluent stream (effluent −2), derived from settling the effluent-1 for 15 min in an Imhoff settler was collected and analyzed as a secondary unit operation. The mean TSS of effluent-2 was 29 ± 19 mg/L (Fig. S1a) equivalent to a 61 % removal efficiency of effluent-1 TSS. Increasing the post treatment settling period (i.e., effluent-2) could further enhance solids separation. The resulting Y_{obs} with this configuration was 1 gCOD produced/g COD consumed while mean SRT was 7.8 days (Table 2). The mean and mode of particle sizes increased during periods of no wastage and conversely decreased during period of biomass wastage. For example, the mean (mode) particle sizes on day 90 and day 150 without wastage increased to 5.14 ± 2.26 mm (0.94 mm) and 4.69 ± 2.52 mm (1.4 mm), respectively (Fig. 4a). These mean and mode sizes decreased to 0.84 ± 1.67 mm (0.22 mm) and 2.18 ± 2.27 mm (0.22) on day 120 and day 250 following bulk wastage period. Bulk wastage of biomass draws out accumulated larger sized OPGs whose growth and development occurs over longer time periods (Abouhend et al., 2020), hence the decreasing mean sizes. The mean SVI_5/SVI_{30} ratio during this period was 1.2 with

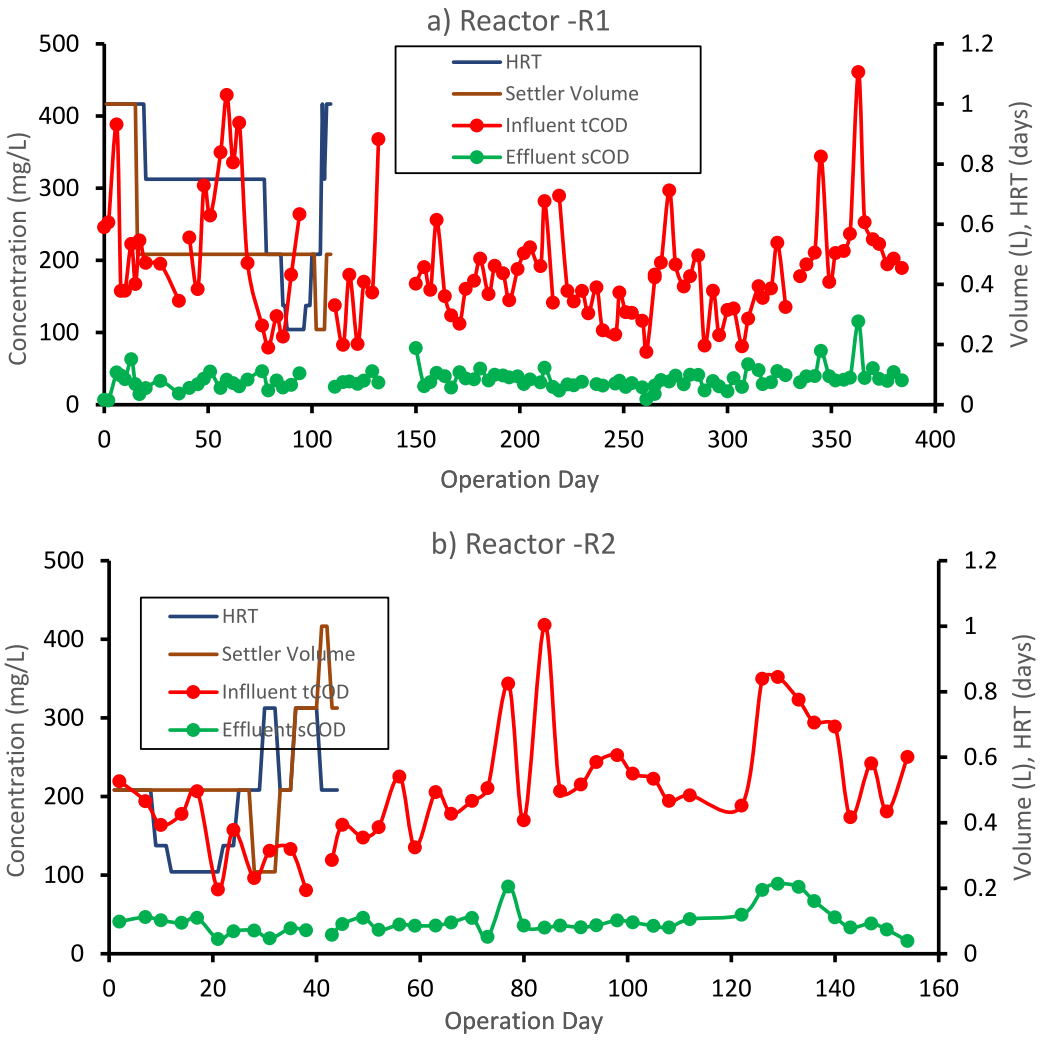

Fig. 3. OPG sCSTR operation of reactor (a) R1 and (b) R2 showing COD fractions (mg/L) of different flow streams at various HRT and internal settler volume configurations. The effluent sCOD is used as a proxy for optimally solids settled effluent from the sCSTR system.

Table 2
sCSTR summary parameters for reactor R1. The operation code indicates the settler–HRT (d)–settler volume (L).

Reactor -R1 Operation Code	Operation days	Y_{obs} (gCOD produced/gCOD consumed)	SRT (days)
$S_{A\text{-}1d\text{-}1L}$	0–36	0.63	7.1
$S_{B\text{-}1d\text{-}1L}$	37–51	0.46	3.0
$S_{B\text{-}1d\text{-}0.5L}$	52–65	0.70	3.5
$S_{B\text{-}0.75d\text{-}0.5L}$: Before wasting	66–226	1.01	6.4
$S_{B\text{-}0.75d\text{-}0.5L}$: With 2 L wasting	227–261	1.40	11.9
$S_{B\text{-}0.75d\text{-}0.5L}$: with 3 L wasting	262–293	0.76	16.7
$S_{B\text{-}0.75d\text{-}0.5L}$	66–272	1.02	7.8
$S_{B\text{-}0.5d\text{-}0.5L}$: With 3 L wasting	272–293	1.00	13.2
$S_{B\text{-}0.5d\text{-}0.5L}$	273–300	0.96	12.5
$S_{B\text{-}0.33d\text{-}0.5L}$	301–307	0.47	2.3
$S_{B\text{-}0.25d\text{-}0.5L}$	308–338	1.22	0.7
$S_{B\text{-}0.33d\text{-}0.5L}$	339–349	1.16	1.2
$S_{B\text{-}1d\text{-}0.5L}$, $S_{B\text{-}0.5d\text{-}0.25L}$	350–384	0.72	2.6
Overall R1 operation	0–384	0.98	5.1

an SVI_5 range of 62–236 mL/g (Fig. 5a).

Fig. 8 shows petri dish images of biomass samples collected from the reactor and indicates an increase in granular size (day 51) and OPG surface smoothening by day 70. Thereafter, detached and significant hairy growth was observed, with visibly green surface growth turning brown by day 180, representing significant growth of diatoms. Notwithstanding, an increase in size and number of OPG biomass and continuous presence of spherical and smooth-surface OPGs (Fig. 8) proliferated by surface layers of cyanobacteria (Fig. 7b) were seen. The hairy granules transformed into a star shaped structure around day 180 (Figs. 7g, 8) persisting through the rest of this configuration ($S_{B\text{-}0.75\ d\text{-}0.5L}$).

High SVI values were observed during periods of biomass wastage and following accidental spill events. Regular daily wastage of 2 L mixed biomass from the reactor from day 230 resulted in a 61 % increase of mean biomass concentrations (Fig. 1a) while mean effluent-1 TSS decreased by 14 % (Fig. 2a). Further MLSS increase occurred with 3 L bulk wastage from day 265 to day 272. The increase in solids inventory from 675 ± 209 mg/L to 1072 ± 262 mg/L and then to 1326 ± 152 mg/L (Fig. 1a) represented a 59 % and 24 % marginal change, respectively. The effluent-1 TSS likewise decreased by 14 % with 2 L wastage compared to the preceding no waste period and by 6 %, with 3 L compared to 2 L wastage (Fig. 2a). Effluent sCOD decreased by 28 % due wastage with no significant difference ($p = 0.56$) between 2 L (24 ± 7 mg/L) and 3 L (25 ± 8 mg/L) wastage schemes (Fig. 3a). In comparison,

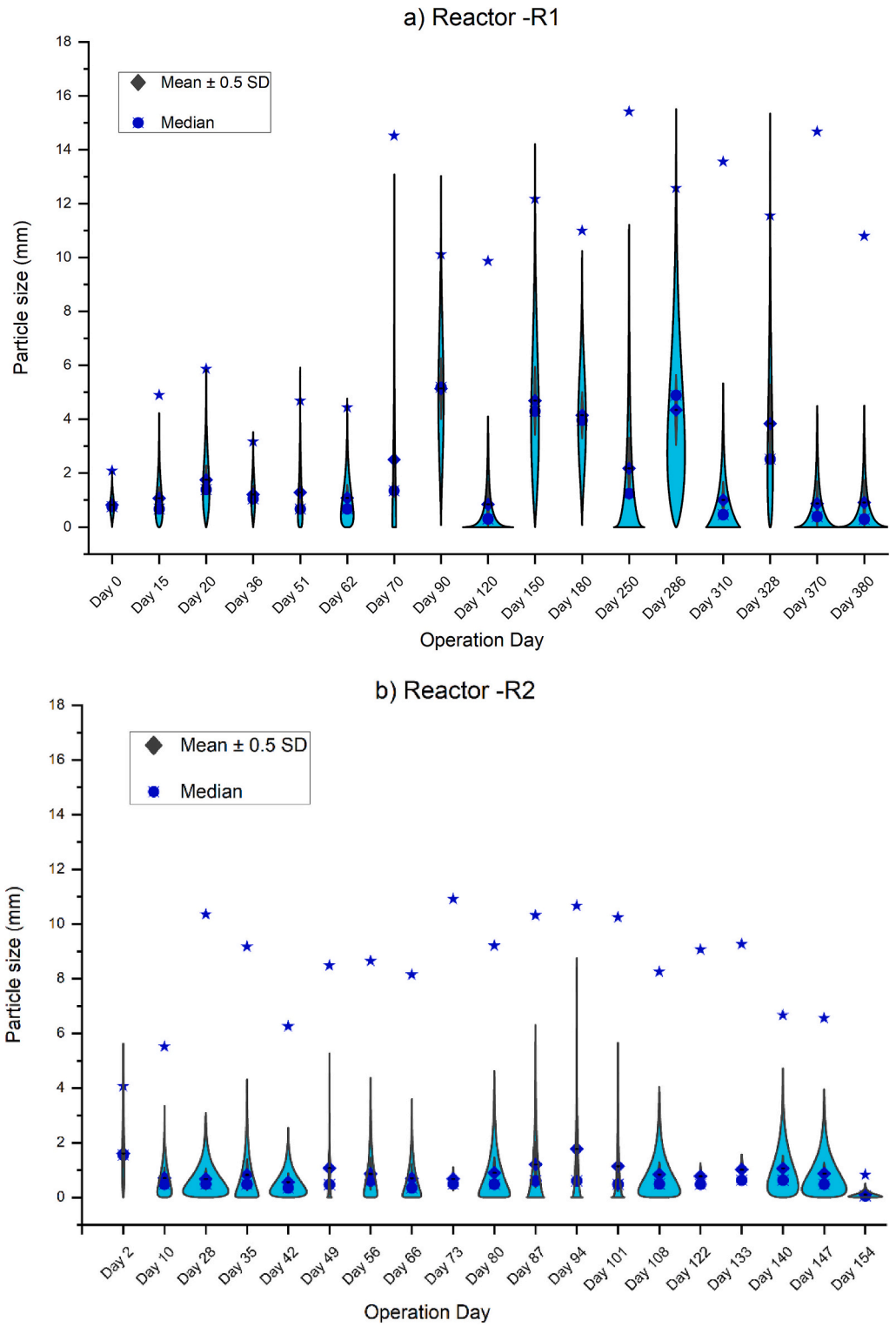

Fig. 4. Particle size distribution (Weibull distribution) of OPG biomass in sCSTR system for reactors (a) R1 and (b) R2. Diamonds and intersect circles on plots show the OPG particles' mean (mm) ± 0.5 standard deviation (SD) and median sizes in each sample, respectively. Stars represent maximum particle sizes.

2 L wastage had the effect on increasing Y_{obs} by 39 % while wasting 3 L decreased Y_{obs} by (27 %) compared to 2 L waste operation (Table 2). Removal of large biomass significantly increased the F:M ratio and enhanced light availability, ingredients requisite for rapid growth of phototrophic biomass in the OPG system. SVI_5 values decreased from 122 ± 50 mL/g before wastage to 62 ± 26 mL/g with 2 L wastage before increasing to 72 ± 20 mL/g with 3 L wastage (Fig. 5a). Secondary solids removal in 15 min settling before wastage was 64 %. This wastage-mediated increase then decrease in SVI_5 is reflected by decreasing removal of effluent-1 TSS of 52 % and 39 % with 2 L and 3 L wastage, respectively (Fig. S1a). In addition to better function from accelerated growth observed with the 2 L wastage scheme, aggregation was enhanced. However, increasing the wastage further resulted in potential net loss of granular biomass, hence deteriorating parameters.

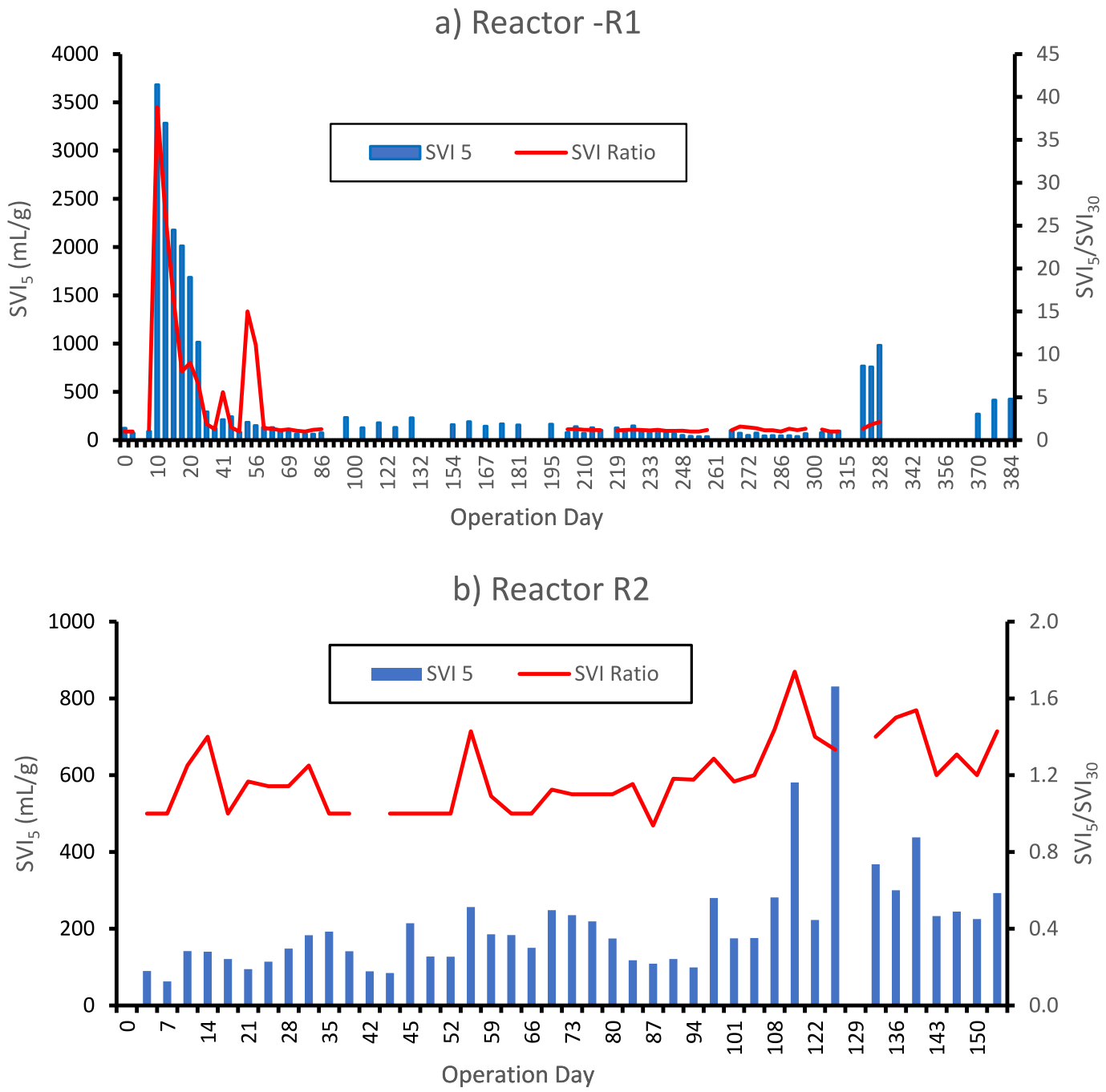

Fig. 5. 5-min sludge volume index (SVI_5) and the ratio of SVI_5 to 30-min SVI (SVI_5/SVI_{30}) for reactors (a) R1 and (b) R2.

TDN removal efficiency increased threefold between 2 L and 3 L wastage schemes and was higher than in the period before wasting (Fig. S 2a). This increase coupled with rapid biomass growth suggests biomass assimilation of nitrogen. Similar, low nitrogen removal efficiencies have been reported for a bio-flocculant algal-bacterial CSTR system (Gutzeit et al., 2005). Abouhend et al. (2018) reported high sensitivity of TDN and NH_4^+ removal to loading rates of organic matter, nitrogen, and ammonia in OPG operated in SBR. Consistent with this report (Abouhend et al., 2018), mean sCOD was higher before wastage (34 ± 11 mg/L) compared to the period with wastage (Fig. S2a).

The biomass with star shaped structure lasted up to day 310 before transition back to green outgrowths (Fig. 7). Chlorophyll-a concentrations were significantly correlated to the biomass VSS with r (88) =0.6 ($p < 0.01$). On the other hand, while chlorophyll-b concentrations showed no significant correlation, r (88) = 0.06 ($p = 0.6$), chlorophyll-c pigments were significantly positively correlated to VSS, r (88) =0.54 ($p < 0.01$). Phycobilisomes on the hand were significantly negatively correlated to the MLVSS trend with r (88) = −0.66 ($p < 0.01$) (Fig. 6a, b).

During the final phases of reactor R1 operation, decreasing the overflow rates via higher HRT ($S_{B\text{-}0.75d\text{-}0.25L}$ and $S_{B\text{-}1d\text{-}0.5L}$) resulted in mean MLSS of 403 ± 42 mg/L (Fig. 1a). The efficiency of TSS removal between effluent-1 and effluent-2 was 71 %, while the mean sCOD was 39 ± 7 mg/L (Fig. 3a).

3.1.2.3. Operation at <0.75 d HRT. From day 272 and on, HRT was decreased further to evaluate higher wastewater treatment loading rate scenarios. This period with 0.5 d HRT and 0.5 L settler volume ($S_{B\text{-}0.5d\text{-}}$

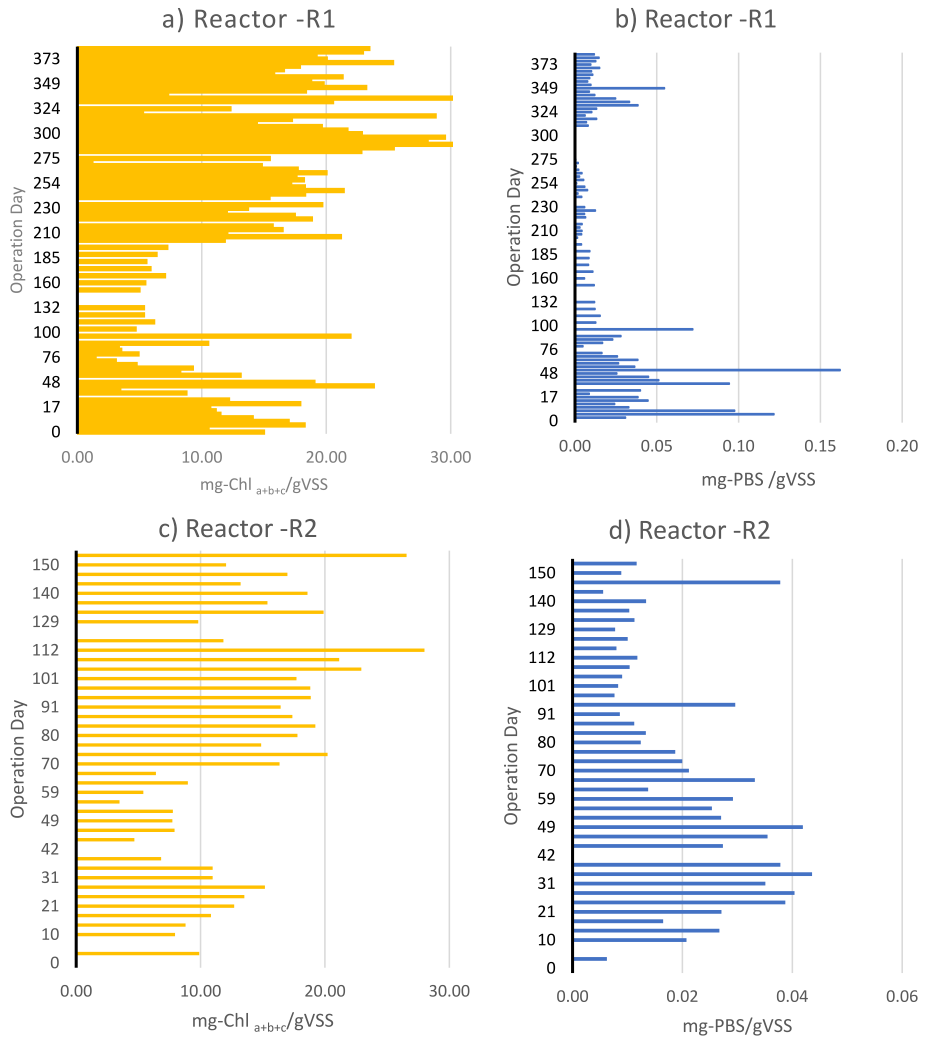

Fig. 6. The level of light harvesting complexes in OPG biomass. Chlorophylls (mg-Chlorophyll $_{a+b+c}$/gVSS) and phycobilisomes (mg-PBS/gVSS) in reactors R1 and R2. (a) Reactor R1 chlorophyll. (b) Reactor R1 PBS. (c) Reactor R2 chlorophyll. (d) Reactor R2 PBS. The phycobilins' maximum concentrations in reactor R2 are four times less than that of reactor R1.

$_{0.5L}$) had the retention time decreased by 33 % (3 min) and overflow rate increased by 50 % compared to that with 0.75-d HRT (Table 1). This operation, which occurred with 3 L bulk biomass wastage, resulted in an increase of MLSS to a peak of 1756 mg/L (mean 1483 ± 155 mg/L) (Fig. 1a). TSS removal efficiency between effluent-1 and effluent-2 decreased to 36 % compared to the 0.75 d HRT operation (Fig. 2a, Fig. S 1a) while the mean effluent sCOD increased to 37 ± 9 mg/L. The equivalent biomass yield was 0.96 gCOD produced/g COD consumed (Table 2) and was accompanied by an increase in mean and maximum particle sizes (Fig. 4a). A general increase in chlorophyll concentrations and decrease of PBS pigment was observed (Fig. 6 a, b) with this MLSS increase.

Operation at 0.5-d HRT without wasting (day 352 to day 366) and 0.5 L settler volume ($S_{B\text{-}0.5d\text{-}0.5L}$) resulted in increasing MLSS, which was reversed with reduced settler volume ($S_{B\text{-}0.5d\text{-}0.25L}$) (Fig. 1a). Moreover, effluent-2 TSS increased during this period with a higher mean (105 ± 8 mg/L) at 0.25 L settler volume compared to 0.5 L volume (97 ± 18 mg/L). Settling efficiency in effluent-2 decreased by 48 % with the decrease in settler volume (Fig. S1a). Increase in sCOD was also observed with reduced settler volume (Fig. 3a).

Further decrease of HRT to 0.33 d ($S_{B\text{-}0.33\ d\text{-}0.5L}$) and 0.25 d ($S_{B\text{-}0.25\ d\text{-}0.5L}$) resulted in drastic biomass loss to mean concentrations of 313 ± 45 mg/L and 224 ± 31 mg/L (Fig. 1a), respectively. This loss can be attributed to too high overflow rates and low retention times within the internal settler. The SVI_5 during this period increased to a maximum of 984 mL/g (Fig. 5a). The open granular structure occurred with growth of hairy biomass (Fig. 7) as well as fine suspended particles, reducing the light availability in the water, which further reduced granulation and water quality via feedback effects.

3.2. Reactor R2 with internal settler S_B

3.2.1. Operation at 0.5 d HRT

Reactor R2 was operated with internal settler S_B at different volumes and HRT settings. Operation at 0.5 d HRT and 0.5 L settler conditions ($S_{B\text{-}0.5d\text{-}0.5L}$), on day 0 to day 24 (Table 1), resulted in a 98 % increase in biomass concentration with a peak of 370 mg/L (mean 216 ± 82 mg/L) (Fig. 1b). Mean effluent-1 TSS concentration was 55 ± 8 mg/L with a 43 % removal efficiency post 15-min settling (effluent-2) (Fig. 2b, Fig. S 1b). The corresponding mean sCOD of effluent during this period was 36 ± 9 mg/L (Fig. 3b) while the yield was 0.89 gCOD produced/gCOD consumed. A low sCOD removal rate (31 %) but high yield alludes to uptake of inorganic carbon from the atmosphere as previously reported (Abouhend et al., 2018; Ji et al., 2022; Trebuch et al., 2023). The SVI_5 during this operation increased to 106 ± 27 mL/g (mean SVI_5/SVI_{30} ratio of 1.1) from an initial 90 mL/g (Fig. 5b). Similar increases in MLSS, comparable yield, decreasing effluent-1 TSS, and comparable sCOD concentrations were observed in reactor R1 operation in similar

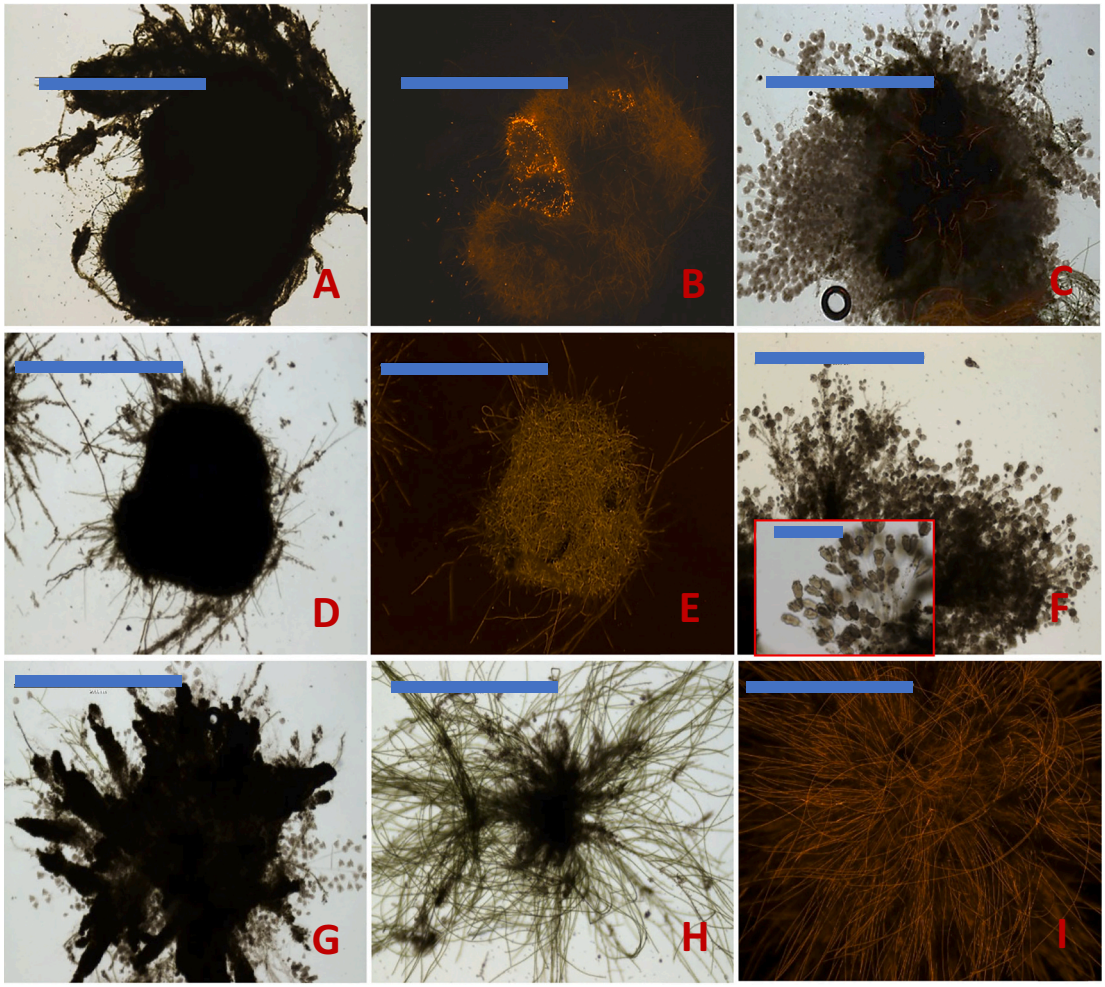

Fig. 7. Microscopy images of photogranular biomass in 50 mL grab-sample mixed biomass from reactors R1 and R2 operated with 50 rpm mixing and 413 ± 53 μmol/m^2-s light intensity. (A) Light microscopy of OPG granule collected from R1 on day 70. (B) Phycobilin autofluorescence of filamentous cyanobacteria within the photogranule shown in (A); break on the cyanobacterial layer may suggest shear rip by impeller blades. (C) Light microscopy image with superimposed fluorescence image of halo granules in R1 observed during periods of sustained high DO. (D) and (E) Light and autofluorescence images of OPG from R2 collected on day 63. (F) Light microscopy image of 'halo granules' in R2 with inset showing a profusion of stalked ciliates on surface. (G) Open structure (star-shaped) granules in R1. (H) Granule with filamentous outgrowths observed during periods of rapid growth in R2. (I) Autofluorescence image of biomass with cyanobacteria growing in hairy form in R1 on day 129, during a period of biomass wastage. Scale bars are 2000 μm and the inset image scale bar is 400 μm.

configuration. The growth of biomass with effective granulation occurred with increase of granular sizes (Fig. 4b), increasing pigment concentrations (Fig. 6 c, d), and smooth granular structures (Fig. 8).

A peak DO of 6.95 mg/L was observed (data not shown) and correlated to rain event on day 81 resulting in dilute influent. Operating at a similar configuration on day 77 to day 87 resulted in increasing biomass inventories by 119 %. In contrast, day 108 to day 122 operation resulted in a 62 % decrease in biomass inventory (Fig. 1b). In both periods, effluent-1 TSS trended upwards while the removal efficiency of solids from this elute increased by 15 % and 9 %, respectively, compared to preceding operation (Fig. 2b, Fig. S 1b). While chlorophyll pigments increased only in the operation between day 77 to day 87, PBS concentrations decreased in both these later 0.5 d HRT configurations. The decrease in light harvesting pigments observed during the day 108 to day 122 period occurred with reduced mean and mode particle sizes of 0.78 ± 0.94 mm and 0.35 mm, respectively by day 122, compared to starting sizes (Fig. 4b).

Decreasing the settler volume at this same 0.5 d HRT ($S_{B\text{-}0.5d\text{-}0.25L}$) resulted in a decrease (27 %) of MLSS concentrations compared to ending concentrations with 0.5 L settler volume (Fig. 1b). While mean effluent-1 TSS levels increased by 46 %, effluent-2 TSS increased by 308 %. This reflects the lower retention time with removal of previously retained slow settling biomass. On the other hand, increasing the settler volume to 1 L and 0.75 L, respectively, resulted in biomass accumulation between day 140 and day 154. This increase to MLSS of 665 ± 102 mg/L was 77 % higher than the mean of the preceding operation (Fig. 1b). Effluent-1 TSS removal with 15 min settling at this higher selector retention time (4.5 min) was 78 % (Fig. 2b, Fig. S 1b). The sCOD had a decreasing trend with a mean sCOD of 28 ± 8 mg/L, which was a 61 % decrease compared to the previous period (Fig. 3b). TDN removal efficiency was highest with the 0.75 L settler volume configuration for 0.5 d HRT operations (Fig. S 2b) suggesting primary removal by biomass assimilation. Decreasing mean SVI_5 values resulted from both settler configurations, compared to previous settings (Fig. 5b) in line with increased mean and maximum particle sizes (Fig. 4b). While the total chlorophyll pigment concentrations increased for both higher and lower settler volumes, a decrease in chlorophyll-c observed at 0.25 L settler volume (data not shown) suggests decreasing diatoms populations. In conformity, phycobilisomes pigments increased at this settler volume, but decreased with 0.75 L settler configuration.

3.2.2. *Operation at <0.5 d HRT*

After the initial 24 days of operation, HRT was decreased to 0.33 d ($S_{B\text{-}0.33d\text{-}0.5L}$) for 7 days then to 0.25 d ($S_{B\text{-}0.25d\text{-}0.5L}$) for 31 days and

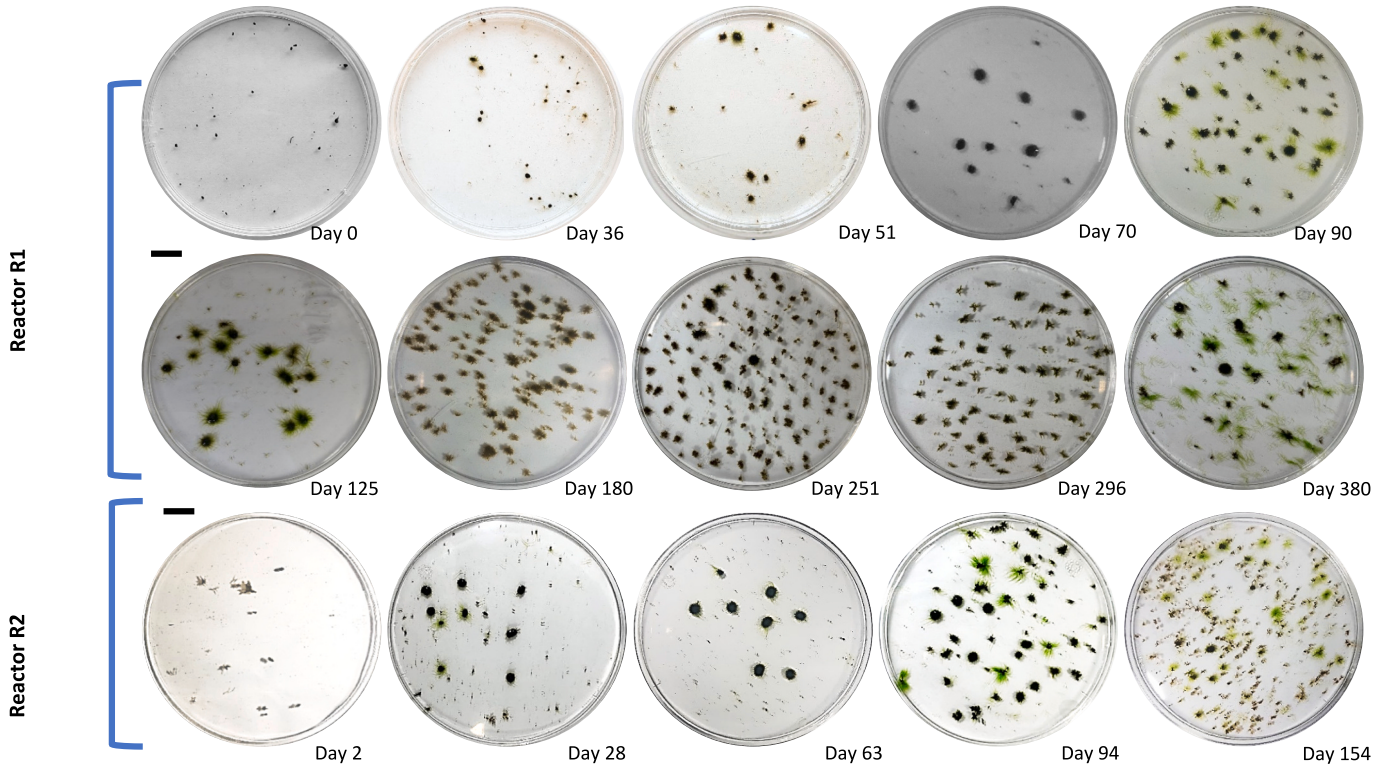

Fig. 8. Petri dish images of mixed biomass grab samples from sCSTR reactors R1 and R2 on different operation days run under different HRT and settler volume configurations shown in Table 1 and detailed in the materials and methods. Reactor R1 samples from day 2 to day 90 were 10 mL each and 50 mL thereafter while all reactor R2 grab-samples were 50 mL. Scale bars are 2 cm.

Table 3
sCSTR summary parameters for reactor R2. The operation code indicates the settler–HRT (d)–settler volume (L).

Reactor -R2 Operation Code	Operation days	Y_{obs} (gCOD produced/gCOD consumed)	SRT (days)
$S_{B\text{-}0.5d\text{-}0.5L}$	0–24	0.89	2.0
$S_{B\text{-}0.33d\text{-}0.5L}$	25–35	0.86	2.0
$S_{B\text{-}0.25d\text{-}0.5L}$	36–66	0.67	1.5
$S_{B\text{-}0.33d\text{-}0.5L}$	67–77	0.75	1.8
$S_{B\text{-}0.5d\text{-}0.5L}$	78–87	N/A	7.0
$S_{B\text{-}0.5d\text{-}0.25L}$	91–94	0.65[a]	4.8
$S_{B\text{-}0.75d\text{-}0.25L}$	95–105	1.22	3.2
$S_{B\text{-}0.5d\text{-}0.5L}$	108–122	1.10	1.9
$S_{B\text{-}0.75d\text{-}0.75L}$	123–140	0.68	3.1
$S_{B\text{-}0.5d\text{-}0.75L}$	141–154	0.96	3.3
Overall R2 operation	0–154	0.81	3.0

[a] Yield covers the entirety of preceding operation period (day 78 to day 94).

back to 0.33 d for 11 days (Fig. 1b, Table 3). This period resulted in mean MLSS of 268 ± 6 mg/L, 339 ± 80 mg/L, and 440 ± 60 mg/L (Fig. 1b), respectively. In addition, mean sCOD initially decreased by 26 % for 0.33 d HRT operations increased by 30 % to 35 ± 6 mg/L for the 0.25 d HRT scheme and further to 44 ± 12 mg/L with ensuing 0.33 d HRT (Fig. 3b). The corresponding yields during this period were 0.86, 0.67, and 0.75 gCOD produced/gCOD consumed (Table 3). Effluent-1 TSS tracked the sCOD trend with sequential separation efficiencies after 15 min of 68 %, 56 %, and 60 % (Fig. 2b, Fig. S 1b). Mean SVI_5 values (SVI_5/SVI_{30}), on the other hand, were 174 ± 19 mL/g (1.1), 147 ± 52 mL/g (1.1), and 234 ± 12 mL/g (1.1) (Fig. 5b). This suggests that intensifying velocity selection by increased feeding regime accelerates growth of slow settling biomass.

3.2.3. *Operation at >0.75 d HRT*

Decreasing the overflow loading rate with high HRT and maintaining a high settling velocity selection with reduced retention time ($S_{B\text{-}0.75d\text{-}0.25L}$) resulted in reduced biomass fluctuations (mean 706 ± 67 mg/L) (Fig. 1b). A period of increasing productivity was observed with high HRT in a low HSP environment ($S_{B\text{-}0.75d\text{-}0.75L}$) akin to that observed with high loading and lower settler selection pressure from day 66 to day 87. Mean SVI_5 increased consistently through these HSP configurations to a peak mean of 448 ± 206 mL/g during the $S_{B\text{-}0.75d\text{-}0.25L}$ operation (Fig. 5b). The increases indicate retention of slow settling particles arising from low flow velocities, despite comparable retention times attained with lower HRT configurations. This in turn indicates significant flow interference to particle settling velocities. This biomass accumulation was also characterized by filamentous detachment (day 122–154) (Fig. 7). Operating at higher retention time and reduced upflow velocities in this instance ($S_{B\text{-}0.75d\text{-}0.75L}$) resulted in a 36 % mean TDN removal efficiency, the highest for all reactor R2 configurations (Fig. S 2b).

Overall, reactor R2 was dominated by smaller particle sizes compared to day 2 sizes as measured by increased skewness and kurtosis over the operation. The mean particle size for reactor R2 operation was 0.82 ± 0.36 mm and an average mode of 0.32 mm (Fig. 4b). Mean particle sizes were observed to increase with biomass concentrations with a peak mean size of 1.77 ± 2.26 mm during the $S_{B\text{-}0.5d\text{-}0.25L}$ operation period (day 94) (Fig. 4b). Between day 2 and day 35, granules increased in size with a maximum size of 10.36 mm on day 10 (Fig. 4b). An increase in particle number was also observed congruent to biomass increase with a peak on day 21. The morphological transition of OPG granules during the operation of reactor R2 is presented in Fig. 7. OPG development was characterized by smooth surfaces up to day 63 with no momentous change in number of larger granules—mean maximum size of 8.07 ± 1 mm (Fig. 4b). This suggests effective settling velocity selection for these rapidly settling granules. Moreover, the number of

particles decreased during this period conceivably due to high HSP and lower settler retention time (1.5 min) employed ($S_{B\text{-}0.25d\text{-}0.5L}$). Filamentous outgrowths on larger OPGs were observed on day 73 to day 101 samples with a marked increase in larger size granules on day 84, and a mean maximum size of 10.26 ± 0.58 mm during this period.

However, granular breakdown was also observed from day 94 with appearance of star shaped OPG biomass occurring with reduced biomass concentrations and mean size 0.78 ± 0.94 mm by day 122. Ensuing operations were characterized by a lower maximum size, mean 4.98 ± 3.05 mm, increasing biomass concentrations (Fig. 1b) and increased hairy growth (Figs. 7, 8). This can be attributed to longer retention resulting from $S_{B\text{-}0.75d\text{-}0.75L}$ (6.75 min) and $S_{B\text{-}0.5d\text{-}0.75L}$ (4.5 min), respectively, increasing the retention of slow growing filamentous microbes. A corresponding increase was observed for all chlorophyll pigments and decrease in phycobilisomes unique to cyanobacteria.

Chlorophyll-a concentration (Fig. 6c) had high positive correlation to biomass concentrations, r (43) =0.82 ($p < 0.01$). Likewise, the trend of chlorophyll-c had a comparable statistically significant correlation, r (43) =0.81 ($p < 0.01$), while chlorophyll-b concentrations had a lower correlation to biomass inventory with r (43) =0.66 ($p < 0.01$). On the other hand, phycobilisomes (Fig. 6d) were significantly negatively correlated to biomass concentrations with r (43) = −0.34 ($p = 0.03$). A rapid initial increase of cyanobacterial phycobilins was observed at lower biomass concentrations up to day 35 (Fig. 6d). The period of PBS increase corresponds to smoother granular surfaces (Fig. 7) and low filamentous outgrowths retained up to day 63. Cyanobacteria (Fig. 8) have been identified as critical to the development of OPGs with microbial layering occurring in tandem with size increases (Abouhend et al., 2020, 2023). Decrease in PBS concentrations on the other hand coincided with appearance of star shaped biomass (Fig. 8) and detached growth. High selection pressures utilized after day 35 resulted in rapid decrease of PBS concentrations (Fig. 6d). Removal of smaller slow settling OPG particles reduces potential for propagation of cyanobacterial laden OPGs. Cyanobacteria have a lower growth rate compared to other photoautotrophs present in the OPG system (Beardall and Raven, 2013; Milferstedt et al., 2017).

4. Discussion

4.1. Reactor functional dependence on HRT and settler volume

The use of algal bacterial aggregates presents opportunities for closing the resource loop in wastewater treatment in addition to offering opportunities for alleviating novel challenges associated with the wastewater treatment processes (Ali et al., 2022; Nagarajan et al., 2020). The cohort of microbes in granular moieties such as OPGs can undertake various bioprocesses essential for wastewater treatment. Primarily, heterotrophic and mixotrophic metabolism reduce organic carbon in the OPG system (Gikonyo et al., 2021b; Gutzeit et al., 2005). Mean effluent sCOD were 31.5 ± 14.3 mg/L and 38 ± 17 mg/L with corresponding sCOD removal rates of 45 % and 41 % for reactors R1 and reactor R2, respectively. The rate of carbon removal was positively correlated to the HRT (r (98) =0.25, $p < 0.001$) and the settler volume (r (98) =0.34, $p = 0.01$), in reactor R1. Likewise, the sCOD removal in R2 had correlations of r (43) =0.33, $p = 0.03$ and r (43) =0.42, $p < 0.01$ to HRT and settler volume, respectively. Failure in low HRT (2 d) lab-scale CFR algal systems has previously been attributed to high organic loading rate (OLR) (Awang and Shaaban, 2016; Wilén et al., 2018). In contrast, no significant correlation was observed between the OLR and COD removal, r (43) = 0.02, $p = 0.87$ and r (43) =0.11, $p = 0.46$ in R1 and R2, respectively. This can be attributed to comparable influence of the HRT and settler volume on biomass velocity selection through overflow velocity and retention time, respectively. The interaction between settler volume and HRT did not significantly impact the COD removal rate ($p = 0.13$) in R1 but was significant in R2 with $p = 0.02$. The 1 L settler volume was identified as the source of statistical influences ($p < 0.001$) in R2.

Total dissolved nitrogen decreased by an average of 12 % for both reactors R1 and R2. This low removal efficiency can be attributed to both low oxygen environment and low SRT maintained during the operation. Gutzeit et al. (2005), operating an algal bacteria system in CSTR with an HRT of 36–60 h, reported a 15 % TN removal, while no ammonia volatilization was observed due to moderate pH values. Comparable pH values were recorded during this operation (6.8 to 7.6). TDN removal was found to relate to biomass inventories suggesting biomass uptake and fixation as the primary removal process. A maximum nitrification level of 5 mg/L/d has also been reported in an enhanced phosphate removal algal-bacteria system with no discernible denitrification (Trebuch et al., 2023). In bench-scale SBR systems, OPGs have been reported to achieve 52 % -57 % TDN removal efficiencies, with up to 96 % of ammonia removal (Abouhend et al., 2018). These reported systems were all operated at longer SRTs, biomass concentration greater than the mean of 0.45 gVSS/L and 0.33 gVSS/L for R1 and R2 and DO concentrations (>0.5 mg/L) achieved in the studied CSTR reactors.

4.2. Organic carbon recovery and yields

High yields observed with a production to consumption ratio of 0.98 gCOD produced/gCOD consumed for reactor R1 and 0.81 gCOD produced/gCOD consumed for reactor R2, underscore the high carbon recovery potential of algal-bacterial aggregates. A Y_{obs} of 1.2 gCOD produced/gCOD consumed has previously been reported for SBR-OPG operations (Abouhend et al., 2018). The observed lower yields compared to this SBR operation, and despite lower operational SRTs can be attributed to light limitation within the sCSTR system. No significant correlation was observed between the solids retention and observed yields ($p > 0.05$). Enhanced biomass production can be detrimental to utility operational budgets but can also be applied to circular WRRF management to enhance production of biomethane and energy generation (Trebuch et al., 2023). While supersaturation of oxygen has been observed in OPG reactors operating under higher light conditions (Gikonyo et al., 2021b), the measured DO during this operation was 1.4 ± 2.1 mg/L and 0.5 ± 0.9 mg/L for R1 and R2, respectively. Oxygen generated at the granular surface is optimally transferred via diffusion gradient for use within the granular matrix. Carbon dioxide is in turn provided by heterotrophic bacteria present in the OPG granules in addition to atmospheric sequestration (Abouhend et al., 2020; Gikonyo et al., 2021b; Milferstedt et al., 2017). The resulting symbiosis fostering microbial codependence is integral to the elastic functionality of granules.

4.3. Considerations for OPG operations using internal settler

Despite its vaunted benefits, continuous wastewater treatment using phototrophic systems would necessitate addition of artificial light to overcome diurnal light cycling. Nonetheless, even with maximum daylight illumination of 2000 μmol/m^2. s (Gikonyo et al., 2021b), light diminution becomes a growth limiting factor in mixed cultures such as OPG systems (Beardall and Raven, 2013). The internal settler unit provides an environment in which particles with settling velocities lower than the operational upflow or overflow velocity are selectively separated and removed out of the system. Literature shows that hydraulic selective pressure (HSP)-based washout can enhance microbial granulation (Beun et al., 1999; Kent et al., 2018; Morgenroth et al., 1997). While OPG can be produced without HSP (Gikonyo et al., 2021a; Park and Takeuchi, 2021), removal of small reactor particles by internal settler HSP or by other means such as size separation reduces preponderance of supra-optimal light conditions. These particles exponentially increase attenuation of incident light in water, impacting photosynthesis, the main driver of the OPG process. However, removal of smaller particles with robust growth can decrease system functional modularity.

OPGs of a between 0.5 and 1 mm have been identified to have highest phototrophic output, and larger layered OPGs with anaerobic zones host denitrifies (Abouhend et al., 2020). Countering this challenge potentially necessitates dedicated treatment zones/reactors to accomplish different treatment objectives with retention time based (settler volume) target selection pressure to accumulate task-specific granular sizes.

In addition, light harvesting occurs at microsecond timescales and at rates 10^6 faster than carbon fixation resulting in electron saturation and photon energy use inefficiency (Beardall and Raven, 2013). To counteract these conditions, an OPG reactor utilizes mixing unit to circulate biomass through different light regimes in the reactors. Higher 'flashing rates'—which may result from increased turbulence as granules traverse through high light to dark regions of the reactor—has been reported to increase productivity of photolithotrophs (Beardall and Raven, 2013). For cyanobacteria which form the structural backbone of OPGs (Milferstedt et al., 2017), growth is strongly correlated to light intensity and weakly to carbon assimilation in a growth optimization strategy (Jahn et al., 2018). The impellers used in these CSTRs exerted a theoretical shear of 0.06 N/m^2. A lower shear force promotes larger sized OPGs while higher shear could be used to limit the size growth of OPGs—if OPG becomes too big, its activity, such as its oxygenic capacity, decreases (Abouhend et al., 2020). Indeed, high shear milieu in an SBR-OPG system was reported to result in higher MLVSS compared to lower shear-lower turnover reactors (Abouhend et al., 2023). Shear positively correlates to higher EPS production, higher COD removals, nitrification, and abundance of cyanobacteria in OPGs (Abouhend et al., 2023). Mixing is therefore essential to ensure optimal interaction of OPGs with light to sustain functional and structural integrity.

While long retention times induce minimal HSP inappropriate for propagation of aerobic granules, short settling durations result in washout of microbes and small granules compromising granulation (Liu and Tay, 2015). Rosa-Masegosa et al. (2021) reported that washing out of slow decanting filamentous microbes is essential to maintain granular integrity in AGS. Decreasing the HRT at constant settler volume increased overflow velocity resulting in biomass purging and shrunk the OPG biomass inventories. A similar TSS decreasing trend was observed with low settler volumes (reduced retention time), at constant HRT. Conversely, biomass was accumulated by increasing HRT or settler volumes. Particle mean sizes increased at the lowest biomass concentration potentially due to selective accumulation of larger sized aggregates with max sizes >1 mm. Due to the relative rigidity of operational HRTs for full scale systems, internal settlers and hydrocyclones can hence be applied to manipulate biomass inventories and achieve OPG functional goals. However, granular transition with these schemes may not be as rapid as reported for SBR operations, due to reduced selection pressures—both feast-famine and HSP. Conventional CSTR systems employ a biomass return system conveying settled biomass back to the reactors. Often achieved with pumping, this can result in granular breakdown due to shear exerted by pump impellers. A CSTR with sludge return of algal-bacterial aggregates was reported to have predominant particle sizes of 400 to 800 μm (Gutzeit et al., 2005). A microscopic exam of the *Chlorella vulgaris* enriched aggregates revealed loose open structures albeit with good settling characteristics. The open structures could be a legacy of breakage during channel transport highlighted in a study (Kent et al., 2018).

Changing from settler S_A to S_B increased the settler overflow velocity 15-fold decreasing biomass inventory in reactor R1 compared to the operation with internal settler S_A. OPGs cultivated in hydrodynamic milieu have been reported to have discrete settling velocities ranging from 3.2 m/h to 75.6 m/h (Gikonyo et al., 2022). Abouhend et al. (2018) reported a maximum zone settling velocity of 14.6 m/h for OPGs grown in SBR. In this sCSTR operation, OPGs retained are also impacted by particle-particle interactions, hence deviating from ideal discrete settling mechanics. These deviations tend to enhance or retard the settling velocity of said particles, potentially the case with large sized OPGs occasionally observed in the effluent (Video 2 attached). In anisotropic flow conditions existing in the internal settler, residual turbulence from mixing can cause a loitering effect. Fast-settling particles may be caught in regions of high upflow velocity or forced vortexes such as induced by the effluent pump, hence impeding their removal (Chen et al., 2020).

Periods of rapid OPG biomass growth were characterized by hairy growth, detachment of filaments and open phenotype. These rapid growth periods occurred with altered F:M ratio arising from intentional wastage, reduced HRT, or accidental loss of biomass by spills. A steady state CSTR system has low substrate, and hence increasing the F:M ratio induces feast conditions with higher substrate fluxes. The observed hairy growth on OPGs and detachment can be attributed to the competitive advantage of disaggregated structures in these feast conditions. Microbial migration from diffusion limited granular morphology into suspended tableau could be responsible for the open and star shaped OPG structures. In addition, high retention durations characteristic of settling velocity selection without biomass wastage, results in accumulation of aged granules. Change of microbial populations has also been identified as a potential cause of old AGS disintegration (Yuan et al., 2017).

Contrary to the uniform substrate gradient expected in this sCSTR operation, OPG reactors have to date been operated with SBR operational cycling, which creates feast and famine conditions (Abouhend et al., 2018). While insufficient as a singular granulation strategy, a substrate feast-famine ratio of 0.5 has been reported as optimal for AGS with higher ratios resulting in disintegration of aerobic granules (Sun et al., 2021). Increased storage of carbon as polyhydroxyalkanoates (PHAs) and glycogen occurs during feast conditions (Fradinho et al., 2021), while subsequent famine enhances substate driven co-aggregation (Kent et al., 2018). Low HRTs of up to 1-h were reported to promote compact AGS in CFR while 3 and 6-h HRTs resulted in filamentous domination. Compaction was also promoted by intermittent feeding in a CFR system. Long retention times, low substrate gradients in bulk liquid, and nutrient deficiency within granules have been reported to cause bulking-inducing filamentous growth in AGS-SBR systems (Liu and Liu, 2006). Over the 384-day and 154-day operations, a structural metamorphosis of the OPGs was observed with granules of assorted sizes. Nevertheless, granulation was sustained indicating potential long-term stability of the process in CFR conditions.

The feast-famine strategy requires augmentation with other selection stresses (Kent et al., 2018; van Dijk et al., 2022). The potential compensatory nature of selection pressures (van Dijk et al., 2022), was briefly evaluated. Shear stress in reactor R2 was doubled with mixing, inducing decreased effluent-2 TSS, improved organics removal and decreasing sCOD. Potential detachment of filamentous outgrowths, increasing the effluent-1 TSS, was accompanied by appearance of compact granules with this change. As indicated earlier, this higher mixing increases flashing rates hence overall phototrophic activity, which coupled with the settler induced hydraulic selection, positively impacting the treatment process. Enhancement of light utility (Beardall and Raven, 2013; Gikonyo et al., 2021b) can be achieved by combining mixing and settling velocity separation of biomass to promote larger inter particle spaces and increase the photic zone in deeper CSTR reactors. Enhancing hydrostatic selection pressure on the other hand with bulk wastage of OPG biomass resulted in increased MLSS level and altered microbial populations. Essential cyanobacteria populations (Abouhend et al., 2023; Milferstedt et al., 2017), were negatively correlated to MLSS. Robust settler ejection of granulating OPGs at rates higher than granulation or growth rates would result in loss of cyanobacteria and system functionality. This potential selecting out of cyanobacteria occurred with increased heterotrophic and algal growth. An overall decrease in phycobilisomes and increasing chlorophyll pigment during the operation merits future causal investigation.

High loading rates- high F:M, results in larger granules with loose structure and influent characteristics impact microbial diversity in specialized niches (Liu and Tay, 2015). For example, high particulate COD is reported to cause filamentous growth and hinder granulation

(Rosa-Masegosa et al., 2021). Low DO environments favor filamentous growth affecting granular stability (Liang et al., 2022). Within the OPG system, only reactor R1 with older OPGs was observed to have correlations between the OLR and chlorophyll-c producing microbial populations. These phototrophs, primarily diatoms, are sensitive to dissolved oxygen concentrations preferentially occupying niche oxygen saturation environment (Fenchel, 2014). Larger retained granules had a halo of stalked ciliates, and their preponderance was related to oxygen concentrations increasing during periods of high residual DO in the sCSTR reactors. Ciliates have chemosensory motility orienting to preferred oxygen gradients (Fenchel, 2014), as evidenced by their OPG exostructural coloniality in high dissolved oxygen tension. Their distribution can also be influenced by availability of prey, bacteria, and algae (Fenchel, 2014), conditions existing during high biomass concentration phases. The ciliates attach to flocs and can form skeletal anchors, key to granular stability (Liang et al., 2022).

Interaction of microbial communities with the environment results in phenotypes existing within a continuum ranging from discrete planktonic cells to complex aggregations, such as flocs, biofilms, and granules (Aqeel et al., 2019; Gikonyo et al., 2021a; Park and Takeuchi, 2021). Ordinarily, while environmental drivers enhance sustenance of dominant morphologies, a blend of morphologies exists in any wastewater culture given the different microbial responses to existing stressors. A full suite of engineered selection pressures, such as those in SBR systems enhance dominant granular structures (Park and Takeuchi, 2021). An amalgam of these selection pressures is requisite with compensation between mechanisms (van Dijk et al., 2022). Operating OPGs at larger scales in SBR resulted in functionally inadequate light interactions (McNair, 2017). Operating in CSTR configurations with steady-state clear bulk liquid coupled with culling of particle sizes using hydraulic selection pressures can optimize light utility. Despite low feast-famine pressure, this sCSTR systems can sustain granular selection pressure, due to selection pressure mechanisms counterbalancing (van Dijk et al., 2022). For photogranular systems, we suggest that cycling of 'light substrate' supplemented by hydraulic selection pressure promote adequate aggregation even in CFR, including CSTR environment. However, singular dependence on hydraulic selection pressure can heighten susceptibility of these CSTR systems to operational changes impacting granular structure.

5. Conclusions

Granular technology for wastewater treatment is coming of age with more widespread applications. Moreover, their potential application in contemporary continuous flow systems presents the next frontier in fully harnessing their potential. For photogranular systems including OPGs, this pursuit must additionally overcome 'light-substrate' limitations arising from particle concentrations and depth related light attenuation. This study examined the utility of internal settlers for the operation of OPGs in CSTR systems. OPGs were sustained and propagated successfully implying overall sustenance of granulation selective pressure. Moreover, manipulation of biomass population to elevate light utility can also be achieved using external selectors such as hydrocyclones. Future research should explore system configuration employing to optimize functionality for these high yield systems amenable to energy resource recovery.

Supplementary data to this article can be found online at https://doi.org/10.1016/j.biteb.2023.101523.

CRediT authorship contribution statement

All the authors contributed to this manuscript in experimental design, running the experiments, or in manuscript writing. **Joseph Gikonyo**: Conceptualization, Data curation, Formal analysis, Investigation, Methodology, Writing – original draft, review & editing. **Ahmed Abouhend:** Investigation, Writing – review & editing. **Andrew Keyser:** Investigation, Data curation, Writing – review & editing. **Yanwen Li:** Investigation, Data curation. **Chul Park:** Conceptualization, Project administration, Supervision, Writing – review & editing.

Declaration of competing interest

The authors declare the following financial interests/personal relationships which may be considered as potential competing interests: Chul Park reports financial support was provided by the National Science Foundation. Joseph Gitau reports equipment, or supplies were provided by both the Amherst Wastewater treatment plant and by the UMASS - Water, Energy and Technology Center. Chul Park has patent pending to UMASS-Amherst. Joseph Gitau has patent pending to UMASS-Amherst. Ahmed S. Abouhend has patent pending to UMASS-Amherst.

Data availability

No data was used for the research described in the article.

Acknowledgments

This work was supported by the NSF PFI (#1919091). The authors would like to thank staff at the Amherst water resource recovery center and Sherrie Webb-Yagodzinski, University of Massachusetts Amherst, for technical support during the experiments and Dr. Sudhir Murthy for technical input in operational testing.

References

Abouhend, A.S., McNair, A., Kuo-Dahab, W.C., Watt, C., Butler, C.S., Milferstedt, K., Hamelin, J., Seo, J., Gikonyo, G.J., El-Moselhy, K.M., Park, C., 2018. The oxygenic photogranule process for aeration-free wastewater treatment. Environ. Sci. Technol. 52, 3503–3511. https://doi.org/10.1021/acs.est.8b00403.

Abouhend, A.S., Milferstedt, K., Hamelin, J., Ansari, A.A., Butler, C., Carbajal-González, B.I., Park, C., 2020. Growth progression of oxygenic photogranules and its impact on bioactivity for aeration-free wastewater treatment. Environ. Sci. Technol. 54, 486–496. https://doi.org/10.1021/acs.est.9b04745.

Abouhend, A.S., Gikonyo, J.G., Patton, M., Butler, C.S., Tobiason, J., Park, C., 2023. Role of hydrodynamic shear in the oxygenic photogranule (OPG) wastewater treatment Process. ACS EST Water. https://doi.org/10.1021/acsestwater.2c00317.

Ahmad, J.S.M., Cai, W., Zhao, Z., Zhang, Z., Shimizu, K., Lei, Z., Lee, D.-J., 2017. Stability of algal-bacterial granules in continuous-flow reactors to treat varying strength domestic wastewater. Bioresour. Technol. 244, 225–233. https://doi.org/10.1016/j.biortech.2017.07.134.

Ali, M., Hong, P.-Y., Mishra, H., Vrouwenvelder, J., Saikaly, P.E., 2022. Adopting the circular model: opportunities and challenges of transforming wastewater treatment plants into resource recovery factories in Saudi Arabia. J. Water Reuse Desalination 12, 346–365. https://doi.org/10.2166/wrd.2022.038.

Ansari, A.A., Abouhend, A.S., Park, C., 2019. Effects of seeding density on photogranulation and the start-up of the oxygenic photogranule process for aeration-free wastewater treatment. Algal Res. 40, 101495 https://doi.org/10.1016/j.algal.2019.101495.

APHA, 2012. Standard Methods for the Examination of Water and Wastewater. APHA, AWWA,WEF, Washington: American Public Health Association.

Aqeel, H., Weissbrodt, D.G., Cerruti, M., Wolfaardt, G.M., Wilén, B.-M., Liss, S.N., 2019. Drivers of bioaggregation from flocs to biofilms and granular sludge. Environ. Sci. Water Res. Technol. 5, 2072–2089. https://doi.org/10.1039/C9EW00450E.

Awang, N.A., Shaaban, M.G., 2016. Effect of reactor height/diameter ratio and organic loading rate on formation of aerobic granular sludge in sewage treatment. Int. Biodeterior. Biodegrad. 112, 1–11. https://doi.org/10.1016/j.ibiod.2016.04.028.

Beardall, J., Raven, J.A., 2013. Limits to phototrophic growth in dense culture: CO_2 supply and light. In: Borowitzka, M.A., Moheimani, N.R. (Eds.), Algae for Biofuels and Energy, Developments in Applied Phycology. Springer, Netherlands, Dordrecht, pp. 91–97. https://doi.org/10.1007/978-94-007-5479-9_5.

Beun, J.J., Hendriks, A., van Loosdrecht, M.C.M., Morgenroth, E., Wilderer, P.A., Heijnen, J.J., 1999. Aerobic granulation in a sequencing batch reactor. Water Res. 33, 2283–2290. https://doi.org/10.1016/S0043-1354(98)00463-1.

Bindhu, B.K., Madhu, G., 2016. Influence of three selection pressures on aerobic granulation in sequencing batch reactor. Indian J. Chem. Technol. 22, 241–247.

Canals, J., Cabrera-Codony, A., Carbó, O., Torán, J., Martín, M., Baldi, M., Gutiérrez, B., Poch, M., Ordóñez, A., Monclús, H., 2023. High-rate activated sludge at very short SRT: Key factors for process stability and performance of COD fractions removal. Water Res. 231, 119610 https://doi.org/10.1016/j.watres.2023.119610.

Chen, Y., Jiang, W., Liang, D.T., Tay, J.H., 2007. Structure and stability of aerobic granules cultivated under different shear force in sequencing batch reactors. Appl.

Microbiol. Biotechnol. 76, 1199–1208. https://doi.org/10.1007/s00253-007-1085-7.
Chen, X., Liu, Z., Chen, Y., Wang, H., 2020. Analytical expression for predicting the reduced settling velocity of small particles in turbulence. Environ. Fluid Mech. 20, 905–922. https://doi.org/10.1007/s10652-019-09731-8.
van Dijk, E.J.H., Haaksman, V.A., van Loosdrecht, M.C.M., Pronk, M., 2022. On the mechanisms for aerobic granulation - model based evaluation. Water Res. 216 (118), 365. https://doi.org/10.1016/j.watres.2022.118365.
Fenchel, T., 2014. Protozoa and oxygen. Acta Protozool. 2014, 3–12. https://doi.org/10.4467/16890027AP.13.0020.1117.
Fradinho, J., Allegue, L.D., Ventura, M., Melero, J.A., Reis, M.A.M., Puyol, D., 2021. Up-scale challenges on biopolymer production from waste streams by Purple Phototrophic Bacteria mixed cultures: A critical review. Bioresour. Technol. 327, 124820 https://doi.org/10.1016/j.biortech.2021.124820.
Gikonyo, J.G., Ansari, A.A., Abouhend, A.S., Tobiason, J.E., Park, C., 2021a. Hydrodynamic granulation of oxygenic photogranules. Environ. Sci. Water Res. Technol. 7, 427–440. https://doi.org/10.1039/D0EW00957A.
Gikonyo, J.G., Keyser, A., Tobiason, J., Jeong, J., Park, C., 2021b. In vivo evaluation of oxygenic photogranules' photosynthetic capacity by pulse amplitude modulation and phototrophic–irradiance curves. ACS EST Eng. 1, 551–561. https://doi.org/10.1021/acsestengg.0c00221.
Gikonyo, J.G., Ansari, A., Park, C., Tobiason, J., 2022. Physical characterization of oxygenic photogranules. Biochem. Eng. J. 186, 108592 https://doi.org/10.1016/j.bej.2022.108592.
Gu, Y., Li, Y., Li, X., Luo, P., Wang, H., Wang, X., Wu, J., Li, F., 2017. Energy self-sufficient wastewater treatment plants: feasibilities and challenges. Energy Procedia 105, 3741–3751. https://doi.org/10.1016/j.egypro.2017.03.868.
Gurung, K., Tang, W.Z., Sillanpää, M., 2018. Unit energy consumption as benchmark to select energy positive retrofitting strategies for Finnish wastewater treatment plants (WWTPs): a case study of Mikkeli WWTP. Environ. Process. 5, 667–681. https://doi.org/10.1007/s40710-018-0310-y.
Gutzeit, G., Lorch, D.P., Weber, A., Engels, M.S., Neis, U., 2005. Bioflocculent algal-bacterial biomass improves low-cost wastewater treatment. Water Sci. Technol. J. Int. Assoc. Water Pollut. Res. 52, 9–18. https://doi.org/10.2166/wst.2005.0415.
He, Q., Chen, L., Zhang, S., Chen, R., Wang, H., Zhang, W., Song, J., 2018. Natural sunlight induced rapid formation of water-born algal-bacterial granules in an aerobic bacterial granular photo-sequencing batch reactor. J. Hazard. Mater. 359, 222–230. https://doi.org/10.1016/j.jhazmat.2018.07.051.
Jahn, M., Vialas, V., Karlsen, J., Maddalo, G., Edfors, F., Forsström, B., Uhlén, M., Käll, L., Hudson, E.P., 2018. Growth of cyanobacteria is constrained by the abundance of light and carbon assimilation proteins. Cell Rep. 25, 478–486.e8. https://doi.org/10.1016/j.celrep.2018.09.040.
Ji, B., Shi, Y., Yılmaz, M., 2022. Microalgal-bacterial granular sludge process for sustainable municipal wastewater treatment: Simple organics versus complex organics. J. Water Process Eng. 46 (102), 613. https://doi.org/10.1016/j.jwpe.2022.102613.
Jimenez, J., Wise, G., Regmi, P., Burger, G., Conidi, D., Du, W., Dold, P., 2020. Nitrite-shunt and biological phosphorus removal at low dissolved oxygen in a full-scale high-rate system at warm temperatures. Water Environ. Res. Res. Publ. Water Environ. Fed. 92, 1111–1122. https://doi.org/10.1002/wer.1304.
Kent, T.R., Bott, C.B., Wang, Z.-W., 2018. State of the art of aerobic granulation in continuous flow bioreactors. Biotechnol. Adv. 36, 1139–1166. https://doi.org/10.1016/j.biotechadv.2018.03.015.
Lauceri, R., Bresciani, M., Lami, A., Morabito, G., 2017. Chlorophyll a interference in phycocyanin and allophycocyanin spectrophotometric quantification. J. Limnol. https://doi.org/10.4081/jlimnol.2017.1691.
Liang, Y., Pan, Z., Guo, T., Feng, H., Yan, A., Ni, Y., Li, J., 2022. Filamentous bacteria and stalked ciliates for the stable structure of aerobic granular sludge treating wastewater. Int. J. Environ. Res. Public Health 19 (15), 747. https://doi.org/10.3390/ijerph192315747.
Liu, Y., Liu, Q.-S., 2006. Causes and control of filamentous growth in aerobic granular sludge sequencing batch reactors. Biotechnol. Adv. 24, 115–127. https://doi.org/10.1016/j.biotechadv.2005.08.001.
Liu, Y., Tay, J.-H., 2002. The essential role of hydrodynamic shear force in the formation of biofilm and granular sludge. Water Res. 36, 1653–1665.
Liu, Y.-Q., Tay, J.-H., 2015. Fast formation of aerobic granules by combining strong hydraulic selection pressure with overstressed organic loading rate. Water Res. 80, 256–266. https://doi.org/10.1016/j.watres.2015.05.015.
Mannina, G., Badalucco, L., Lorenzo, B., Cosenza, A., Trapani, D.D., Gallo, G., Laudicina, V.A., Marino, G., Muscarella, S.M., Presti, D., Helness, H., 2021. Enhancing a transition to a circular economy in the water sector: the EU project WIDER UPTAKE. Water 13, 946. https://doi.org/10.3390/w13070946.
McNair, A., 2017. Pilot reactor operation of the oxygenic photogranule (OPG) wastewater treatment process. In: Environ. Water Resour. Eng. Masters Proj. https://doi.org/10.7275/2rc1-qw06.
Milferstedt, K., Kuo-Dahab, W.C., Butler, C.S., Hamelin, J., Abouhend, A.S., Stauch-White, K., McNair, A., Watt, C., Carbajal-González, B.I., Dolan, S., Park, C., 2017. The importance of filamentous cyanobacteria in the development of oxygenic photogranules. Sci. Rep. 7 (17), 944. https://doi.org/10.1038/s41598-017-16,614-9.
Morgenroth, E., Sherden, T., Van Loosdrecht, M.C.M., Heijnen, J.J., Wilderer, P.A., 1997. Aerobic granular sludge in a sequencing batch reactor. Water Res. 31, 3191–3194. https://doi.org/10.1016/S0043-1354(97)00216-9.
Nagarajan, D., Lee, D.-J., Chen, C.-Y., Chang, J.-S., 2020. Resource recovery from wastewaters using microalgae-based approaches: a circular bioeconomy perspective. Bioresour. Technol. 302 (122), 817. https://doi.org/10.1016/j.biortech.2020.122817.
Obaideen, K., Shehata, N., Sayed, E.T., Abdelkareem, M.A., Mahmoud, M.S., Olabi, A.G., 2022. The role of wastewater treatment in achieving sustainable development goals (SDGs) and sustainability guideline. Energy Nexus 7 (100), 112. https://doi.org/10.1016/j.nexus.2022.100112.
Park, C., Takeuchi, N., 2021. Unmasking photogranulation in decreasing glacial albedo and net autotrophic wastewater treatment. Environ. Microbiol. 1462–2920, 15780. https://doi.org/10.1111/1462-2920.15780.
Puyol, D., Batstone, D.J., Hülsen, T., Astals, S., Peces, M., Krömer, J.O., 2017. Resource recovery from wastewater by biological technologies: Opportunities, challenges, and prospects. Front. Microbiol. 7, 2106. https://doi.org/10.3389/fmicb.2016.02106.
Qin, L., Tay, J.-H., Liu, Y., 2004. Selection pressure is a driving force of aerobic granulation in sequencing batch reactors. Process Biochem. 39, 579–584. https://doi.org/10.1016/S0032-9592(03)00125-0.
Regmi, P., Sturm, B., Hiripitiyage, D., Keller, N., Murthy, S., Jimenez, J., 2022. Combining continuous flow aerobic granulation using an external selector and carbon-efficient nutrient removal with AvN control in a full-scale simultaneous nitrification-denitrification process. Water Res. 210 (117), 991. https://doi.org/10.1016/j.watres.2021.117991.
Rosa-Masegosa, A., Muñoz-Palazon, B., Gonzalez-Martinez, A., Fenice, M., Gorrasi, S., Gonzalez-Lopez, J., 2021. New advances in aerobic granular sludge technology using continuous flow reactors: engineering and microbiological aspects. Water 13, 1792. https://doi.org/10.3390/w13131792.
Safitri, A.S., Hamelin, J., Kommedal, R., Milferstedt, K., 2021. Engineered methanotrophic syntrophy in photogranule communities removes dissolved methane. Water Res. X 12 (100), 106. https://doi.org/10.1016/j.wroa.2021.100106.
Sengar, A., Basheer, F., Aziz, A., Farooqi, I.H., 2018. Aerobic granulation technology: laboratory studies to full scale practices. J. Clean. Prod. 197, 616–632. https://doi.org/10.1016/j.jclepro.2018.06.167.
Smetana, G., Grosser, A., 2023. The oxygenic photogranules—current progress on the technology and perspectives in wastewater treatment: a review. Energies 16, 523. https://doi.org/10.3390/en16010523.
Smol, M., 2022. Chapter 1 - circular economy approach in the water and wastewater sector. In: Stefanakis, A., Nikolaou, I. (Eds.), Circular Economy and Sustainability. Elsevier, pp. 1–19. https://doi.org/10.1016/B978-0-12-821,664-4.00018-2.
Stauch-White, K., Srinivasan, V.N., Camilla Kuo-Dahab, W., Park, C., Butler, C.S., 2017. The role of inorganic nitrogen in successful formation of granular biofilms for wastewater treatment that support cyanobacteria and bacteria. AMB Express 7, 146. https://doi.org/10.1186/s13568-017-0444-8.
Sun, Y., Angelotti, B., Brooks, M., Wang, Z.-W., 2021. Feast/famine ratio determined continuous flow aerobic granulation. Sci. Total Environ. 750, 141467 https://doi.org/10.1016/j.scitotenv.2020.141467.
Trapote, A., Albaladejo, A., Simón, P., 2014. Energy consumption in an urban wastewater treatment plant: the case of Murcia Region (Spain). Civ. Eng. Environ. Syst. 31, 304–310. https://doi.org/10.1080/10286608.2013.866106.
Trebuch, L.M., Sohier, J., Altenburg, S., Oyserman, B.O., Pronk, M., Janssen, M., Vet, L.E. M., Wijffels, R.H., Fernandes, T.V., 2023. Enhancing phosphorus removal of photogranules by incorporating polyphosphate accumulating organisms. Water Res. 119, 748. https://doi.org/10.1016/j.watres.2023.119748.
Whitman, W.B., Rainey, F., Kämpfer, P., Trujillo, M., Chun, J., DeVos, P., Hedlund, B., Dedysh, S. (Eds.), 2015. Bergey's Manual of Systematics of Archaea and Bacteria, 1st ed. Wiley. https://doi.org/10.1002/9781118960608.
Wilén, B.-M., Liébana, R., Persson, F., Modin, O., Hermansson, M., 2018. The mechanisms of granulation of activated sludge in wastewater treatment, its optimization, and impact on effluent quality. Appl. Microbiol. Biotechnol. 102, 5005–5020. https://doi.org/10.1007/s00253-018-8990-9.
Xu, D., Li, J., Liu, J., Qu, X., Ma, H., 2022. Advances in continuous flow aerobic granular sludge: a review. Process. Saf. Environ. Prot. 163, 27–35. https://doi.org/10.1016/j.psep.2022.05.018.
Yuan, S., Gao, M., Zhu, F., Afzal, M.Z., Wang, Y., Xu, H., Wang, M., Wang, S.-G., Wang, X., 2017. Disintegration of aerobic granules during prolonged operation. Environ. Sci. Water Res. Technol. 3 https://doi.org/10.1039/C7EW00072C.
Zhang, C., Sun, S., Liu, X., Wan, C., Lee, D.-J., 2017. Influence of operational conditions on the stability of aerobic granules from the perspective of quorum sensing. Environ. Sci. Pollut. Res. 24, 7640–7649. https://doi.org/10.1007/s11356-017-8417-7.